Russian Chemical Reviews **76** (6) 583 – 598 (2007) © 2007 Russian Academy of Sciences and Turpion Ltd

DOI 10.1070/RC2007v076n06ABEH003708

Multinuclear magnetic resonance imaging as a multifunctional tool for the investigation of the properties of materials, transport processes and catalytic reactions

I V Koptyug, A A Lysova, K V Kovtunov, V V Zhivonitko, A V Khomichev, R Z Sagdeev

Contents

I.	Introduction	583
II.	Multinuclear magnetic resonance imaging of solids	583
III.	Multinuclear magnetic resonance imaging of transport processes	585
IV.	Magnetic resonance imaging of chemical reactions	588
V.	Conclusion	595

Abstract. New physicochemical applications of multinuclear magnetic resonance imaging that will determine the development of the method in the near future are considered. These include studies of solids, investigations of mass transfer processes in multiphase systems, studies on *in situ* reactors, heterogeneous hydrogenation with para-hydrogen and spectroscopy of long-lived singlet states. It is noted that in addition to an extension of the range of objects and processes of interest, the magnetic resonance imaging technique itself undergoes considerable changes. The bibliography includes 204 references.

I. Introduction

Magnetic resonance imaging (MRI) formerly referred to as nuclear magnetic resonance (NMR) tomography is known primarily as a method of medical diagnostics. This method is also widely used in biological studies. At the same time, MRI has found increasing and fruitful application in studies of nonliving objects, including investigations in chemistry, chemical engineering, materials science, *etc*.[1–4] Both the fundamentals of MRI and its physicochemical applications were considered in the reviews.[5–7] In the last five years, this method has gained new applications due to its extensive development, resulting in a considerable expansion of the range of objects and processes studied by MRI. This range includes catalytic reactors and biofilm reactors, fuel cells, microreactors, polymers, drug delivery systems, gas hydrates, rock cores, building materials, film coatings, cultural heritage objects, plants, food products, *etc*. This, in turn, stimulates the further development of MRI technique itself. Efforts of researches in this field of science led to fundamentally new applications, including those, which have been considered to be impossible or impracticable. In particular, these are MRI of gas transport, single-spin magnetic resonance, NMR spectroscopy and MRI in highly inhomogeneous or very low magnetic fields, MRI of solids and high-temperature processes, the diffusion coefficient and flow rate measurements at time intervals that are substantially longer than the spin relaxation times, and many other.

Unfortunately, these investigations have received little attention in Russia. The present review summarises recent achievements and trends in the development of MRI, including results obtained in recent years at the International Tomography Centre of the Siberian Branch of the Russian Academy of Sciences. In the present review, we do not try to cover the results of all investigations. This is practically impossible taking into account the progress achieved in this field in the last 5 – 10 years. Our aim is to attract the attention of researchers to this field of science by presenting the most remarkable applications, which apparently will determine the progress in MRI in the nearest future.

II. Multinuclear magnetic resonance imaging of solids

In biomedical applications, the MRI technique is mainly used for investigations of soft tissues and fluid transport (blood and lymph fluid) in living organisms. Until recently, scientific and technical applications of MRI have been limited mainly to investigations of objects containing considerable amounts of liquids. The progress in MRI of gases is hampered mainly by a low density of gases (*i.e*., a low concentration of nuclear spins) and, as a consequence, low sensitivity and low spatial resolution. As a result, MRI of gases has found limited use although methods for the preparation of hyperpolarised gases with a considerable degree of nuclear spin polarisation have been extensively developed in recent years to overcome limitations associated with low sensitivity. At the same time, in spite of a relatively high density of solid materials, their investigations by MRI also present difficulties due mainly to the characteristic features of magnetic resonance of solids. However, it is evident that the use of MRI for investigations of solid materials would substantially extend the scope of this method.

In the solid phase (unlike in liquids), anisotropic interactions involving nuclear spins are not averaged to zero because of low molecular mobility. This is responsible for a large linewidths in NMR spectra of solids. For example, the line-

I V Koptyug, A A Lysova, K V Kovtunov, V V Zhivonitko, A V Khomichev, R Z Sagdeev International Tomography Centre, Siberian Branch of the Russian Academy of Sciences, ul. Institutskaya 3a, 630090 Novosibirsk, Russian Federation. Fax (7-383) 333 13 99,
tel. (7-383) 333 35 61, e-mail: koptyug@tomo.nsc.ru (I V Koptyug),
lysova@tomo.nsc.ru (A A Lysova),
kovtunov@tomo.nsc.ru (K V Kovtunov),
v_zhivonitko@tomo.nsc.ru (V V Zhivonitko),
khomichev@tomo.nsc.ru (A V Khomichev),
tel. (7-383) 333 14 48, e-mail: itc@tomo.nsc.ru (R Z Sagdeev)

Received 2 April 2006
Uspekhi Khimii **76** (6) 628 – 645 (2007); translated by T N Safonova

widths for quadrupolar nuclei are often >1 MHz. An exception are soft solids, such as polymers and elastomers, which can often be studied by conventional MRI techniques.[8,9] For rigid solids, a large linewidths lead to a very fast NMR signal decay, resulting in a substantial decrease in the sensitivity of the technique. Moreover, the NMR signals cannot be detected at all in some cases. In addition, magnetic field gradients, which are far beyond the possibilities of commonly used 'liquid-phase' instruments, may be required to achieve a satisfactory spatial resolution. For example, separate two-dimensional images of powdered alumina and zeolite[10,11] and one-dimensional projections of ceramic samples[12] were obtained from ^{27}Al NMR signals with the use of magnetic field gradients amplitude of 225–350 G cm^{-1}. However, even such values are beyond the possibilities of modern NMR tomographs.

Several research teams are currently developing approaches to MRI of solids based on solid-state NMR techniques,[7] such as magic-angle sample spinning,[13] the use of multiple-pulse sequences,[14] large magnetic field gradients,[15–18] single point imaging (SPI), single point ramped imaging with T_1 enhancement (SPRITE),[19–21] continuous wave NMR,[22] *etc*. However, the wide application of MRI of solids is substantially hampered by the necessity (actual or implied) of the use of specialised instruments and complex techniques;[23] the vast majority of commercial or homebuilt instruments are oriented towards procedures conventionally used in NMR and MRI of liquids.

It is known that a line broadening in NMR spectra of solids is inhomogeneous, *i.e*., broadened signals are virtually sets of overlapping signals with a substantially smaller own width. This fact can be used in different ways. For example, the use of long frequency-selective pulses can allow excitation of only a part of the inhomogeneously broadened resonances. In this case, the time of transverse magnetisation decay T_2^* is substantially increased and it becomes possible to use liquid-phase techniques in MRI of solids.[24,25] The obvious drawback of this approach is that only a small part of nuclear magnetisation is used in experiments, resulting in low sensitivity.

In our studies,[26–30] we used another approach. Originally, the choice of a solid material (γ-Al_2O_3) and, consequently, the magnetic nucleus (^{27}Al) was determined by our MRI studies of heterogeneous hydrogenation of unsaturated compounds on Pt/γ-Al_2O_3 or Pd/γ-Al_2O_3 catalysts and by the fact that alumina is a commonly used support for catalysts. However, we found that this approach is also applicable to many magnetic nuclei involved in rigid solid materials. Our investigations were based on a number of concepts well-known in the field of NMR. First, a large difference between homogeneous and inhomogeneous widths of the signals is essentially a large difference between the characteristic decay time of the observed signal T_2^* (the time of transverse magnetisation decay or free induction decay) and the true transverse magnetisation relaxation time T_2. After the application of the first non-selective radio frequency (RF) pulse, a rapid signal decay with the characteristic time T_2^* is observed. However, the application of the second RF pulse can substantially reverse the decay and refocus magnetisation.[12] Second, the central transition ($1/2 \leftrightharpoons -1/2$) in the spectrum of half-integer quadrupolar nuclei $I = (2n+1)/2$, $n = 1, 2\ldots$, including ^{27}Al ($I = 5/2$), is much narrower than the satellite transitions.[18,31] Therefore, the detection of the central band in the spectra of quadrupolar nuclei in many cases poses no big problems,[32,33] in particular if combined with the phase encoding of the spatial information.

The above approach was used with advantage for two-dimensional imaging of cylindrical alumina pellets and alumina or cordierite monolithic honeycomb supports with ^{27}Al NMR signal detection.[26,27,29] The images were acquired within ~15 min. To demonstrate the potential of this method, a series of composite samples of complex composition containing various materials (Al_2O_3, V_2O_5, $KMnO_4$, $NaHCO_3$, glass, *etc*.) were prepared. Images of the corresponding parts of the composite samples at a spatial resolution of 150–300 μm were obtained by detecting signals of different nuclei (^{27}Al, ^{23}Na, ^{51}V, ^{55}Mn).[28–30]

The observation of a signal from a glass tube in images obtained from the ^{27}Al NMR signal is evidence that multinuclear MRI shows promise for investigation of glass samples. The studies were dased on the detection of NMP signals of ^{27}Al, ^{11}B, ^{23}Na, and ^{29}Si NMR nuclei.[26,29,30] This can be used, for example, in studies of the macrostructures of catalysts and supports, glass and ceramic materials and the structures of granular layers and containers in which they are located. In particular, the structure of a reactor can be visualised in studies of catalytic processes occurring in the reactor. This, along with studies of transport processes, will allow investigation of the correlation between the structure of the reactor and the processes that take place in it. For this purpose, the MRI technique was used for three-dimensional imaging of model granular layers composed of glass beads (^{23}Na MRI, Fig. 1) or spherical alumina grains (^{27}Al MRI).

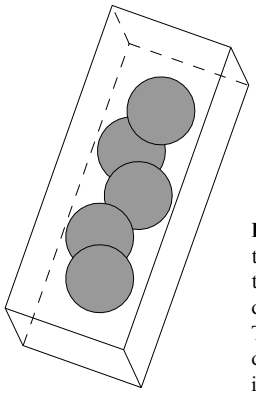


Figure 1. Three-dimensional image of the packing of glass beads with a diameter of 3.5 mm in a glass tube with an inner diameter of 4.2 mm.
The image was acquired within 9 h by detecting the ^{23}Na NMR signal. The image of the tube has been removed.

The merit of the MRI method is that it not only provides structural information but, which is more important, also gives spatially resolved maps of properties of the objects of interest (velocity, temperature, chemical composition, *etc*.). Hence, the further progress in MRI of solids will be directed towards the use of this method with different image contrast mechanisms. An evident field of application involves studies of the motion of solids and granulated materials.

The development of spatially resolved NMR thermometry is another promising area of investigation. Heat transport processes are of primary importance in the design and use of catalytic reactors. Nuclear magnetic resonance tomography is rather widely applied in thermometry of liquids.[7,34–37] However, none of the available approaches based on the signal detection of a liquid phase can be used for thermometry of heterogeneous catalytic processes. This is associated with the fact that all parameters used in NMR thermometry (signal intensity, chemical shifts, relaxation times, diffusion coefficients) substantially depend on other factors, for example, on the amount of a liquid in pores. Therefore, it is impossible to relate unambiguously the changes in these parameters to the changes in temperature.

At the same time, the detection of a signal from a solid matrix, which is much less subjected to changes during operation of a reactor, allows the use of MRI for thermometry of reactors. This possibility was documented almost exclusively for soft solids. For example, the pronounced temperature dependence of the longitudinal (spin–lattice) and transverse (spin–spin) nuclear relaxation times (T_1 and T_2, respectively) was used to construct three-dimensional temper-

ature maps for a *cis*-polybutadiene block, through which cold and hot water was pumped using two pipes,[38] and for vulcanisates of butadiene – styrene rubber under dynamic mechanical load.[8, 9, 39] Two-dimensional MRI of a KBr crystal,[40] for which the time T_1 of the ^{81}Br NMR signal shows a pronounced temperature dependence, is an example of thermometry of rigid solids. As mentioned above, alumina is widely used for the preparation of catalysts and supports. Investigations demonstrated that both the time T_1 and the amplitude of the ^{27}Al signal of alumina are characterised by a pronounced temperature dependence.[26] In the future, it can be used for the development of procedures for spatially resolved NMR thermometry of solids.

III. Multinuclear magnetic resonance imaging of transport processes

Magnetic resonance imaging has long been advantageously used in investigations of transport processes.[6] In particular, liquid flow, filtration, dispersion and diffusion in various geometries, including transport in model granular layers,[41–44] plants,[45, 46] electroosmotic flow,[47, 48] turbulent flows,[49] *etc*., were considered in a vast number of publications.

Nowadays, MRI is being increasingly used in studies of structures of bioreactors and transport processes in them. The development of new technologies based on the use of various bioreactors is of importance, for example, in such fields as waste water treatment, food industry, construction of artificial tissues, *etc*. The MRI technique allows the non-invasive determination of the amount and spatial distribution of a biomass in a reactor and location of inhomogeneities in biofilm structures. For example, studies of the growth of biopolymers based on *Staphylococcus epidermidis* in a capillary bioreactor showed the presence of clusters of biomass, in which channels and cavities were distinguished.[50] The use of relaxation time contrast made it possible to obtain separate three-dimensional MRI images of water and biopolymers.[51]

Another approach to the separate visualisation of water and biofilms was used in the study,[52] where the differences in the diffusion coefficients were employed. The MRI method was applied also to investigate the structures of methanogenic aggregates from an anaerobic purification system of waste water.[53] The contrast of MRI images is substantially enhanced upon absorption of paramagnetic compounds by a biofilm.[54–56] In model studies, the removal of metal ions (La^{3+} and/or Cu^{2+}) from aqueous solutions with biopolymers based on the bacterium *Citrobacter sp*. was investigated.[55, 56] Considerable attention was focussed on the flow and diffusive transport in bioreactors.[50, 54, 57, 58] The flow in a new coaxial bioreactor based on hollow fibre permeable membranes was studied.[59] The relationship between the structure and transport properties of biopolymers was considered in several publications.[50, 58] Mammalian cell-based bioreactors have found increasing use for the production of antibodies, hormones and proteins for therapeutic and clinical application, the tissue growth for transplantation and the design of artificial tissues and organs. The distribution and transport of paramagnetic gadolinium complexes in such reactors were investigated.[60, 61] Aspects of application of MRI in studies of transport and biological activity in biofilms and bioreactors were considered in several reviews (see, for example, Refs 62 and 63).

In recent years, considerable attention has been given to application of MRI in studies of two-phase (liquid – gas) flows in various geometries,[64] in particular, of gas and liquid trickle flow in model granular beds. In this case, MRI experiments provide information on the residual and dynamic liquid holdup in a reactor, the presence of liquid streamlets in the bed and wetting of the catalyst surface. For example, it was demonstrated[65] that the flow pattern can remain unchanged for many hours for a co-current trickle flow of water and air in a model granular bed at constant gas and liquid flow rates. An analysis of the results of investigation was used for the determination of the above-mentioned parameters and their dependence on the liquid flow rate. Changes in the gas flow rate do not lead to substantial changes in the liquid distribution in the layer. However, the initial state of the granular bed was found to have a substantial effect on the gas and liquid distribution in the bed.[65, 66] A study of the dependence of the liquid holdup in the reactor and wetting of the surface of cylindrical alumina pellets in a granular bed on the liquid flow rate[67] showed that smaller grains are characterised by higher values of these parameters. After the flow is turned on as well as after the temporary interruption of the liquid feed, a few minutes[64, 68] to several hours[69] are required for the establishment of the stationary liquid and gas distribution in the bed.

Investigations of fast dynamic processes under two-phase flow conditions require fast MR imaging. The imaging at a rate of 10 images per second revealed liquid slugs passing through the imaged slice at a high liquid flow rate.[64, 68] Ultrafast imaging (20 ms for two-dimensional images and 0.3 s for three-dimensional images) allows MRI studies of gas – liquid two-phase flows in the trickle, pulsing and transient flow regimes.[70, 71] Most likely, the pulsing regime begins with the appearance of local fluctuations and is characterised by the coexistence of regions with constant and fluctuating contents of a liquid. The sizes of the regions with an unstable flow increase with the liquid flow rate and finally the regions coalesce. In the transient flow regime, the instability regions in the bed are shifted, which is apparently responsible for a hysteresis in the plot of the pressure drop *vs*. the liquid flow rate. In the pulsing flow regime, changes in the intensity of most of elements of an MR image are observed. To characterise the periodicity of changes in the local liquid content in the bed, the time autocorrelation function was calculated from these data. A preliminary study of the periodic mode with a modulated liquid feed to the bed was documented.[70] In spite of changes in the liquid distribution in the bed after the liquid flow rate returns to the starting value, no changes in the wetting of the catalyst and the liquid holdup in the bed were observed.

It should be noted that the character of transport and its quantitative characteristics can be radically changed if the mass transfer is coupled with heat transfer and/or a chemical reaction (see Section IV.2). A comparative study of a two-phase flow of a diesel oil and N_2 in a bed of glass beads or alumina trilobes was carried out under normal conditions and at high temperature and pressure (398 K, 10 atm).[72] The liquid holdup in the bed was determined from MR images. The results obtained in the trickle flow mode showed a considerable influence of the temperature on the dynamic liquid holdup in the bed, which decreases with temperature.

To study a two-phase flow in channels of honeycomb monolithic supports, for example, in a bubble-train flow with alternating liquid slugs and gas bubbles, it is also necessary to use fast magnetic resonance imaging because, unlike a steady-state pattern in the trickle flow mode, the gas and liquid distribution pattern is continuously changed. The possibility of acquiring 4–8 successive two-dimensional images in $\sim$0.6 s was demonstrated in studies of air – water two-phase bubble-train flow in a thin pipe[73] and a cordierite monolithic honeycomb support.[74, 75] These experiments allow one to determine the size of gas bubbles and liquid slugs and to follow their motion in time. A fast NMR signal decay provides indirect evidence for liquid recirculation in the case of two-phase bubble-train flow.[73] The same approach was used in studies of ascending gas bubbles in channels of a monolith placed in a static liquid.[64, 66, 67, 76]

Studies of the filtration of liquid – liquid two-phase systems in porous media, for example, of water and silicon oil embedded in glass beads, are presently underway.[77, 78]

The possibility of investigating gas flow and filtration by the MRI technique has been demonstrated earlier.[79–82] The results of these studies gave impetus to further progress in MRI techniques as applied to investigations of gas transport. For example, a methane flow and accumulation of solid particles in soot filters of diesel engines was considered.[83] A relatively high spatial resolution (100 – 250 μm) was achieved by increasing the gas pressure to 10 MPa. The measured maps of gas flow velocity showed that the flow distribution through a porous filter wall is relatively uniform along the channel length. The next series of experiments was concerned with the accumulation of small carbon particles, which were introduced into a gas flow, in a filter.

Until recently, it has been believed that the turbulent gas flow in an inhomogeneous magnetic field should lead to fast NMR signal decay and, consequently, this flow cannot be studied by MRI. However, recently it has been demonstrated that this is not true. The maps of flow velocity and turbulent diffusivity for SF_6 flowing at velocities > 10 m s^{-1} (Re $> 10^5$) above a step or about a wing model were reported.[84] The experimental results are in rather good agreement with calculations by computational fluid dynamics methods.

Even at high pressure, the sensitivity in experiments on MRI of gases remains substantially lower than that of MRI of water. Hence, velocity maps can be obtained only in channels of a rather large diameter and, in contrast to MRI of liquids, cannot be obtained in granular beds. However, studies of gas filtration in porous media are of considerable interest in many fields of science and technology. The use of pulsed field gradient NMR (PFG NMR) for measuring an average propagator (the velocity distribution of molecules) holds promise as an approach to studying gas flow and filtration.[79, 81, 85] This method was used to obtain average propagators for axial and transverse directions of propane or butane flows in different granular beds.[86, 87] If the time between gradient pulses (Δ), during which the molecular motion is determined, is short, the Gaussian distribution with a maximum for the zero displacement is observed. A relatively large width of this distribution is associated with a large gas diffusion coefficient. As Δ increases, an extended wing on the side of larger displacements appears in the axial displacement distribution. Then a Gaussian distribution is formed again but with a maximum near the average displacement due to gas flow. The widths of the axial and transverse distributions for large Δ are determined by the corresponding dispersion coefficients, which are substantially larger than the gas diffusion coefficient. In experiments, the dependence of the axial and transverse dispersion coefficients on Δ, the gas flow rate and the grain size in the bed was studied. The Gaussian distribution at large Δ for the axial transport indicates that dead zones are absent in the layer. In the case of gas filtration through a bed of porous particles [for example, of poly(vinyl chloride)],[87] the axial distribution shows the second peak at zero displacements in the limit of large Δ. This peak corresponds to the gas present in grain pores, which is rather slowly exchanged with the free flowing gas. In addition, the characteristic autocorrelation times of the velocity of gas molecules were experimentally studied for filtration through model granular bed.[88]

In spite of the progress in application of MRI in studies of gas transport, low sensitivity is still the main obstacle to such investigations. Hence, considerable recent attention has been focussed on the production of hyperpolarised gases with a considerable increase (by several orders of magnitude) in nuclear spin polarisation compared to thermal equilibrium polarisation in a spectrometer or tomograph magnet field.[89] Laser procedures were developed for the continuous generation of hyperpolarised noble gases (^{129}Xe, ^{3}He, ^{83}Kr).[90–92] It is convenient to use these procedures to study gas flow and filtration by MRI.[80, 93]

The use of hyperpolarised gases, particularly combined with highly sensitive methods for the signal detection (for example, with a superconducting quantum interferometer) allows the detection of NMR signals and MR imaging at very low magnetic fields using extremely small field gradients. For example, experiments [94] were carried out at a magnetic field of 2.3 mT, which is approximately 3 orders of magnitude lower than those used in most of MRI studies of non-living objects. In the cited study, the filtration of hyperpolarised ^{129}Xe* through an aerogel and a bed of powdered polypropylene was considered. In the latter case, due to a large chemical shift difference (200 ppm or 5 Hz), bulk xenon and adsorbed xenon were distinguished in spite of a very low magnetic field. Ultra-low frequency magnetic fields allow investigation of samples inside a metal container.[95] In strong magnetic fields, these investigations are in principle impossible because high-frequency electromagnetic radiation does not penetrate into conducting screens (skin-effect).

In recent years, methods of the so-called remote-detection NMR and MRI have been developed based on the use of continuous generation systems of hyperpolarised gases and their delivery.[96–99] The remote detection is a new method, in which spatial information is encoded into an NMR signal with the use of radiofrequency pulses and field gradients at the moment when molecules (information carriers) are present in the object of interest, while the signal is detected at a different site. This provides delay for the time of molecule transport from the object to the site of detection. The distance between the object of interest and the site of detection can vary from several millimetres to several metres if the transport time is no longer than the spin relaxation time, which determines the lifetime of the encoded information. An obvious advantage of this approach is that conditions of signal detection can be optimised regardless of the properties and size of the object of interest. Preliminary studies using remote-detection NMR have demonstrated an enhancement of sensitivity and spatial resolution for hyperpolarised ^{129}Xe* in model objects and real porous materials.[96, 97] The remote signal detection was applied in MRI of transport in model microreactors.[98, 99] This made it possible to perform detailed studies on the role of flow, diffusion and mixing processes and reveal dead zones.[99]

The transport of solid granulated materials is used in many industrial processes, including fluidised granular beds, granulation, drying, pneumatic transport, *etc*. Magnetic resonance imaging is widely used for investigating such processes. However, all MRI studies of the transport of solids are based on the detection of the NMR signal of a liquid phase. Hence, liquid-containing solid particles are required. Plant seeds (poppy or mustard) with high oil and moisture content, pharmaceutical pellets with a liquid core, and liquid-saturated porous grains are often used for this purpose.[4, 6, 100, 101]

Three-dimensional images of a granular bed fluidised with an air stream [102] clearly show low-density regions (as vertical columns) of the particle distribution above each orifice of the gas-distribution plate. Interestingly, these regions were observed at a gas velocity lower than the minimum fluidisation velocity ($U < U_{mf}$). At $U > U_{mf}$, these regions coalesce into a single low-density region in the upper part of the bed. The images also clearly show dead zones between adjacent orifices. Mixing of particles in a fluidised bed was studied using two types of particles, which give and do not give NMR signals.[103] Different modes of fluidisation were examined by recording axial profiles of the particle density distribution, the particle velocity distribution and the effective dispersion coefficient.[104] In somewhat more complex MRI experiments, the contributions of coherent (differences in particle velocity) and incoher-

ent (velocity modulation due to collisions) particle motion to the dispersion coefficients can be distinguished.[105] In particular, the dispersion coefficients for the transverse transport with and without considering the coherent contribution differ by a factor of 3–4; for the axial transport, this difference is substantially smaller. Local information on the particle velocity averaged over the time and an element of an MR image can be obtained by combining MRI sequences and velocity encoding methods.[102, 105] Velocity distribution maps reflect the upward particle motion in the central part of the bed and downward motion in the near-wall region at a much lower velocity. The transport of a gas used for fluidisation of a granular bed can be studied by MRI. The gas exchange between different phases (gas bubbles and emulsions) was studied and gas velocity distributions at different gas flow rates were obtained with the use of hyperpolarised xenon.[106, 107]

Magnetic resonance imaging is applied also to study fluidisation of a granular bed in vibrating containers.[108–111] In addition, the particle transport in Couette flow[112, 113] and in horizontal rotating cylinders was investigated[114–117] and filtration of mineral oil-containing Al_2O_3 particles through a bead pack, which serves as a model of a catalytic reactor, was studied.[85, 118, 119]

The drawback of the above-considered applications of MRI in studies of the transport of solids is that it is necessary to detect the signal of a liquid phase. This largely limits the range of materials and processes, which can be studied by this method. Until recently, the possibility of detecting the NMR signal of a solid phase in such studies has not been considered. The successful use of multinuclear MRI allowed us to study for the first time the motion of solids by the direct detection of the NMR signal of a solid phase. We used[30] the MRI method for visualising the rotation of a cylinder filled with an alumina powder. Three-dimensional velocity maps of the two velocity components perpendicular to the cylinder axis were constructed by detecting the ^{27}Al NMR signal. These data are in good agreement with the results of calculations based on the known parameters, *viz.*, the rotation velocity and the diameter of the sample. Propagators for motion of finely grained alumina under the force of gravity were also obtained (Fig. 2).

The further progress in applications of MRI is greatly hampered by the sensitivity of the method. This is also true for the MRI of solids, especially when the signals of nuclei with a low natural abundance of a magnetic isotope or a low magnetogyric ratio are detected. Hence, we made considerable efforts to enhancing the sensitivity of detection of the ^{27}Al NMR signal and signals of other nuclei. One of approaches in

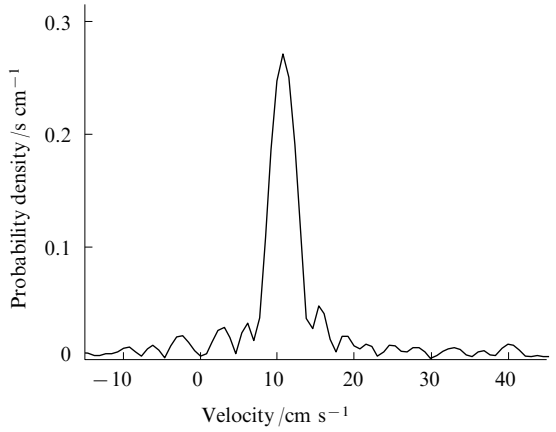


Figure 2. Particle velocity distribution of finely grained Al_2O_3 in a vertical pipe obtained by detecting the ^{27}Al NMR signal.

NMR of half-integer quadrupolar nuclei is based on an increase in the level population difference of the central transition as a result of a inversion of satellite transitions by means of adiabatic sweep of the radiofrequency field.[120] This made it possible to double the intensity of the ^{27}Al NMR signal in MR imaging of a glass tube with a wall thickness of 1.5 mm.[30] The use of a narrower spectral band in the signal detection[19, 121] led to a further increase in the signal-to-noise ratio by a factor of 3.5. Nowadays, we use another approach based on the development and construction of higher-sensitivity resonator-type radio frequency detectors.

Multinuclear MRI can be useful not only in studying the transport of solids but also in investigating the transport of different dissolved compounds. From a methodological viewpoint, this obviates problems associated with the detection of signals of a solid phase because a fast molecular motion in solutions averages anisotropic nuclear spin interactions, resulting in a narrowing of NMR lines by several orders of magnitude. Due to this, all liquid-phase MRI techniques are fully applicable for multinuclear MRI of solutes.

Transport processes of dissolved substances have attracted interest of researchers in different fields of science and technology. For example, the transport of salts in porous building materials is of primary importance. In recent years, multinuclear MRI has found application in studies of such processes.[122, 123] The design of functional porous materials is often based on impregnation of a porous matrix with various substances. For example, efficient sorbents were prepared by introducing different salts into pores of alumina, silica gel or another porous matrix.[124] It will be possible in future to characterise both transport processes of dissolved substances in impregnation and drying steps and the final distribution of a solid-phase component introduced into a porous matrix after complete removal of the solvent by combining MRI of dissolved compounds and MRI of solids.[29, 125, 126]

The transport of dissolved substances is of great importance also in the preparation of supported catalysts by impregnation of a porous support with the corresponding solutions. The diffusive transport rate of substances into a porous support substantially depends on the character of interactions between these substances and the support, the presence of modifying additives in solution, pH of the medium and other factors. In some case, this rate can be very low, but in this case uniform distribution of an active component over a support cannot be achieved. In some cases, a non-uniform distribution of egg-shell, egg-white, *etc.* types are required. In earlier studies, we have found that platinum hexachloride ($PtCl_6^{2-}$) deposited onto an extended surface of alumina can increase the proton spin relaxation times of liquids filling the pore space of supports.[127, 128] As a result, MRI images reflecting the macrodistribution of platinum in grains was obtained by detecting signals of a liquid (cyclohexane or water) in grain pores. Analogous experiments were performed for palladium tetrachloride ($PdCl_4^{2-}$). Moreover, the non-destructive character of MRI allowed, for the first time, the observation of the dynamics of redistribution of adsorbed platinum hexachloride in real time in one grain in the course of competitive adsorption from a solution together with oxalic acid.[127, 128] Unlike $PtCl_6^{2-}$ and $PdCl_4^{2-}$, paramagnetic adsorbates lead to a decrease in the spin relaxation times of contacting liquids. This allows the use of MRI in studies of simultaneous adsorption of two active components of different nature (for example, $PtCl_6^{2-}$ and Cu^{2+}) upon simultaneous deposition onto an alumina grain.[118, 129]

More recently, studies of practical importance were carried out. The corresponding procedures were developed using alumia-supported (Ni/Co)Mo catalysts for hydrodesulfurisation. These catalysts are often prepared with the addition of other components, *viz.*, co-promoters and modifying agents

(for example, phosphates and citrates). The transport of phosphate in an alumina grain upon impregnation of the latter in an aqueous H_3PO_4 solution was studied in the first step. Magnetic resonance imaging with ^{31}P NMR signal detection provided dynamic visualisation of the phosphate transport in a grain in the course of impregnation.[125, 126] To confirm the reliability of this method, maps of the spatial distribution of phosphate in the solid phase were recorded after termination of impregnation at various stages of impregnation and the subsequent drying of the granules. This became possible due to the development of the above-considered (see Section II) multinuclear MRI of solids. The distribution of phosphate in a dry grain was demonstrated to correlate with the distribution of phosphate in the liquid phase during impregnation. In addition, an investigation with the use of the initially dry grain combined with an alternating detection of ^{31}P (phosphate) and ^{1}H (water) images demonstrated fast capillary ingress of water from a solution, the penetration of phosphate inside the grain being much slower due to a strong interaction between the phosphate and the surface of alumina pores.

In the next step, the cobalt transport during impregnation of an alumina pellet with an aqueous solution of a cobalt salt was investigated. The dynamics of the process was studied by MR imaging by detecting ^{1}H NMR signal of water because paramagnetic cobalt ions (Co^{2+}) have a substantial effect on the intensity of the NMR signal of water. The addition of citric acid to an impregnation solution was demonstrated to have a substantial effect on the impregnation process: the cobalt concentration at the periphery of the grain decreases due to a stronger interaction between citric acid and the pore surface and the displacement of cobalt further into the granule (Fig. 3). The influence of the impregnation conditions on the character of cobalt transport and the final distribution of cobalt over the grain of the support was studied in detail. For example, the redistribution of cobalt in the course of impregnation at high and low pH (8 and 1, respectively) of an impregnation solution for a grain with a diameter of 3.5 mm is completed in ~ 2 h. At pH 1, the final distribution has an egg-yolk type. At pH 8, cobalt is uniformly distributed over a granule in spite of the presence of citrate. At intermediate pH (for example, 5), the impregnation time exceeds 15 h. Images obtained by MRI in studies of the transport of Co^{2+} ions were converted into concentration profiles with the use of calibration curves, *i.e.*, it was demonstrated that quantitative information on transport processes in the course of supported catalysts preparation can be obtained.

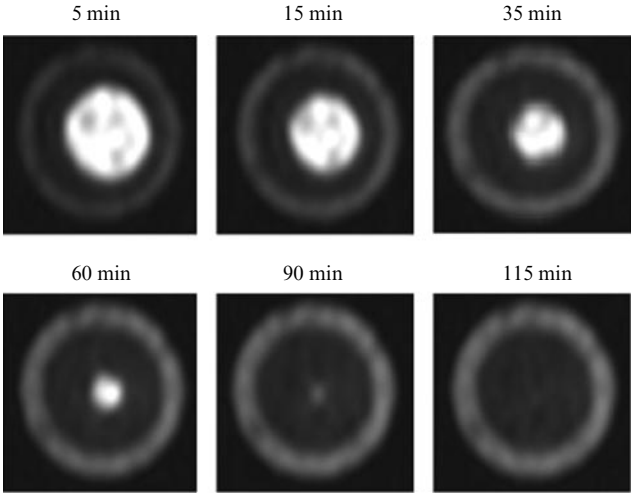


Figure 3. Two-dimensional ^{1}H MRI images reflecting the dynamics of transport of Co^{2+} ions into a γ-Al_2O_3 grain in the course of its impregnation with a solution of 0.2 M $Co(NO_3)_2$ and 0.4 M citric acid at pH 1.
The images were acquired by detecting the ^{1}H NMR signal; the dark ring corresponds to the part of the grain with the highest concentration of Co^{2+} ions; the spatial resolution was (139×231) μm^2.

In the next step, the transport of molybdenum ($Mo_7O_{24}^{6-}$) was studied. Granules were impregnated with an aqueous solution of ammonium heptamolybdate. Diamagnetic molybdenum ions (Mo^{6+}) were found to lead to a substantial increase in the spin relaxation times of water in the pores. This effect is analogous to the effect used earlier in studies of impregnation of support grains with an aqueous solution of H_2PtCl_6 or H_2PdCl_4 (see above). Based on the results of these investigations, approaches were developed for selective visualisation of the regions of grains containing (or not containing) Mo^{6+}, and a procedure was devised for observing the dynamics of molybdenum transport in grains during impregnation. However, it is necessary to use MRI in combination with other physicochemical methods for complete characterisation of such multicomponent systems. For example, spatially resolved optical spectroscopy can be used for determining the nature of ionic metal complexes.[126, 130]

In the above-described investigations, the transport of a diamagnetic precursor of an active component in grains of a support in the course of the preparation of supported catalysts by impregnation was for the first time monitored by detecting directly the NMR signal of the metal atom. This was exemplified [125] by the preparation of a Pt/γ-Al_2O_3 catalyst with the observation the dynamics of the process by detecting the ^{195}Pt NMR signal. The approaches developed in the latter study were used for investigating the preparation of catalysts on other supports, for example, for studying the distribution of an active component in different samples of monolithic honeycomb supports both after calcination and in freshly prepared samples.[131] To visualise the spatial distribution of an active component, T_1-weighted images were generated. Therefore, approaches were devised for the first time to using MRI for the non-destructive control of the preparation of supported catalysts by dynamic visualisation of the distribution of active components and compounds promoting catalytic activity.

IV. Magnetic resonance imaging of chemical reactions

1. Homogeneous reactions

Under homogeneous conditions, a liquid-phase reaction or related mass-transfer processes can give rise to non-uniform spatial distributions of reactants, products, intermediates and other important parameters. In these cases, MRI can provide useful information on processes occurring in systems. An example is MRI studies of the Belousov–Zhabotinsky (BZ) reaction, metal ion-catalysed oxidation of organic substrates by bromate anions.[132] A series of interesting MRI investigations were carried out in this field [133, 134] (see the review [7]). In the last three to four years, after a hiatus, interest in this problem was rekindled. For example, the reaction alternative to the classical BZ reaction, *viz.*, the non-catalytic cyclohexane-1,4-dione + bromate + acid reaction, was studied.[135] However, since the MR image contrast in all previous studies of the BZ reaction has been based on the periodic change in the oxidation state of metal ions (catalyst), the latter investigation was performed with the addition of manganese ions as a passive indicator of the processes occurring in the system. This allowed investigation of the appearance and evolution of wave structures in this system. The concentrations of the reactants, products and intermediates at different instants of time were determined by NMR monitoring of the reaction, which partially confirmed the reaction mech-

anism proposed earlier. Later,[136] spatial maps of the concentrations of Mn(II) and Mn(III) ions were obtained directly in the course of the BZ reaction.

The BZ reaction is homogeneous. However, its behaviour can be substantially changed by performing this reaction in thin capillaries or in an inert porous medium. The behaviour of the BZ system in glass bead or quartz sand packs was investigated.[88, 137, 138] In particular, the concentration wave velocity in a glass bead pack with a bead diameter of 0.5 mm was demonstrated to decrease by a factor of $\sim$2.5 after passing through the interface between the bulk liquid and the granular layer filled with the liquid. The wave velocity is proportional to the square root of the diffusion coefficient of an autocatalyst.[132] The diffusion coefficient in a porous medium decreases by a factor of ε/T (ε is the porosity of the medium and T is the tortuosity of the pore space) compared to the diffusion coefficient in the liquid bulk.[139] Estimates demonstrated that changes in the concentration wave front velocity after passing through the interface between these phases are associated primarily with this factor.

The concentration wave propagation velocity decreases as the curvature of the front increases.[140, 141] As the critical curvature is achieved, the formal velocity becomes negative, resulting in the disappearance of wave activity of the medium. The local (on the length scale of individual pores) curvature of the wave front is determined by the pore size in a granular layer. Hence, the propagation of the concentration front can be influenced by varying the grain size. In particular, at fixed concentrations of the key reactants, there is a critical pore size, below which no wave activity is observed. In addition, the wave propagation velocity depends on the bromate anion concentration.[132] These investigations actually demonstrated that each granular layer is characterised by a particular concentration range, where the wave activity can be observed. For porous materials with small pores, such as alumina, the wave activity was not found at all.

Considerable attention is given to characteristic features of coupling of a non-linear chemical reaction with transport processes in open systems. In particular, very interesting effects are observed in the course of filtration of a BZ reaction medium through inert granular layers. The descending wave velocity (*i.e.*, the wave propagating in the direction of flow) in a porous medium was demonstrated to be substantially larger than the sum of the flow velocity and the wave velocity in the stationary medium, whereas the ascending wave can remain steady-state in a laboratory reference system in a wide range of flow velocities.[137, 142, 143] Spatially resolved periodic-in-time concentration oscillations were studied[144] by pumping the BZ reaction medium through a glass bead pack. To create constant boundary conditions at the layer inlet, the reaction mixture was introduced from a continuously stirred tank reactor. After the initial transition period, stationary wave structures were observed in the system over a long period of time. Evidently, it is impossible to detect three-dimensional wave structures by optical methods in a non-transparent system.

Since the detailed mechanism of the BZ reaction is rather complex, this unusual behaviour of wave fronts in a granular layer in the presence of a reactant flow remains to be explained.

The concentration wave propagation is observed also in different non-oscillating autocatalytic reactions, which often have a much simpler mechanism than the BZ reaction. In this connection, we performed a series of investigations of such reactions to reveal the common features of coupling of transport processes with a non-linear reaction. For experiments in a reactor containing a stationary granular layer, we chose two autocatalytic systems suitable for MRI studies: oxidation of the Co^{2+} ethylenediaminetetraacetate (EDTA) complex by hydrogen peroxide[145] (OH^- ions act as the autocatalyst)

$$2\,CoEDTA^{2-} + H_2O_2 = 2\,CoEDTA^- + 2\,HO^-,\ pH\ 4 \qquad (1)$$

and oxidation of Fe^{2+} with nitric acid (NO_2^- ions act as the autocatalyst)

$$2\,Fe^{2+} + HNO_3 + 2\,H^+ = 2\,Fe^{3+} + HNO_2 + H_2O. \qquad (2)$$

In addition to the above-mentioned advantages, an advantage of these systems over the BZ system is that the initiation of chemical waves can easily be controlled. Owing to changes in paramagnetic properties of metal ions in the course of the above transformations, it is easy to acquire MR images with T_1 contrast. For reaction (1), a qualitative pattern for the chemical wave front propagation was obtained. In experiments with reaction (2), the quantitative dependence of the wave propagation velocity on the flow velocity of the reactants through a stationary granular layer was measured. These experiments demonstrated that the wave velocity linearly depends on the flow velocity of reactants, but the slope of the plot differs from unity, *i.e.*, the wave velocity in the moving medium is not a simple sum of the wave velocity in a stationary medium and the flow velocity. For comparison, reaction (2) was performed in a thin capillary. The latter process is characterised by a liquid flow velocity distribution, but the dependence of the wave propagation velocity on the average reactant flow velocity is analogous to that observed for reaction (2) in a reactor with a stationary granular layer. The experiments demonstrated that the wave front propagation can be accompanied by a spontaneous change in velocity from slow to fast and back. This unusual behaviour is apparently attributed to the exothermic character of the chemical reaction and, consequently, to changes in the density of the reaction solution.

In these experiments, considerable efforts were made to develop MRI techniques for studying the chemical wave propagation under different conditions. For example, the chemical wave propagation in polymeric media is of interest as a model, which can be used to study living biological tissues, where different specific transformations can proceed. To perform experiments in polymeric media, we chose oxidation of thiosulfate with chlorite ions

$$S_2O_3^{2-} + 2\,ClO_2^- + H_2O = 2\,SO_4^{2-} + 2\,Cl^- + 2H^+. \qquad (3)$$

This reaction shows a wave activity at low (< 0.1 mol litre^{-1}) concentrations of the reactants (autocatalysis by H^+ ions). Isopropylacrylamide gel was used as a polymer matrix. We found that the nuclear spin relaxation times of water vary with pH. For example, the chemical wave propagation in the gel impregnated with the chlorite–thiosulfate reaction solution led to a change in pH by 7 units, resulting in an increase in the relaxation time T_1 by $\sim$200 ms. This allowed us to acquire MR images with pH contrast of the propagating wave front at different instants of time.

The spatially resolved NMR thermometry for visualisation of the chemical wave propagation is another area of methodological development. Since reaction (3) is exothermic, the concentration front propagation can in principle be observed from changes in the local temperature of the medium. Magnetic resonance imaging is rather widely used for measuring the local temperature in different samples.[7] For systems containing large amounts of water, including living objects, the temperature determination is often based on an almost linear temperature dependence of the chemical shift of a water molecule in a wide temperature range. For the first time, we used MRI thermometry for measuring the local temperature in the course of concentration wave propagation.[146] The reaction was performed in a vertical glass cell with an inner diameter of 9 mm, and two-dimensional images of a 2-mm thick slice were acquired at three-second intervals for central longitudinal or transverse sections. As a result, temperature profiles for this colourless reaction were obtained (Fig. 4). According to the

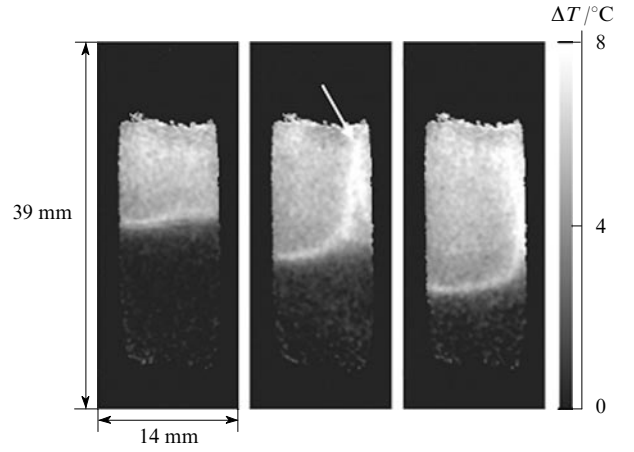


Figure 4. Temperature profiles obtained in the course of chemical wave propagation in a chlorite – thiosulfate system.
Longitudinal sections of the cell are shown; the images were acquired at 25-s intervals; the convective flow is indicated by an arrow.

MRI data, an increase in the temperature of the solution in the course of reaction front propagation was ~8 °C, which is in good agreement with the results of thermocouple measurements performed separately. The accuracy of MRI measurements of the temperature in these experiments was estimated at 1 °C. After the front propagation, the temperature of the solution gradually decreases to the initial level, which is reflected in the temperature profiles. These profiles also demonstrate the presence of convective flows in the cell, resulting from heating of the medium in the vicinity of the reaction front. Therefore, the above-described procedures are applicable to studies of the influence of reactant transport in polymeric media and the temperature on the chemical wave propagation.

2. Heterogeneous reactions

The application of MRI in the *in situ* studies of operating reactors is a relatively new field that made its appearance in the 21th century.[147] Nevertheless, numerous data were obtained during this short period of time. Investigations carried out in the course of a reaction are of great importance because coupling of transport processes with reactions and attendant processes (heat transfer and phase transformation) can fundamentally change the situation.

First *in situ* MRI investigations of heterogeneous catalytic reactions proceeding at high temperature were carried out at the International Tomography Centre of the Siberian Branch of the Russian Academy of Sciences in collaboration with the Institute of Catalysis of the Siberian Branch of the Russian Academy of Sciences. Heterogeneous hydrogenation of unsaturated compounds (α-methylstyrene, heptene, and octene) on supported metal catalysts ($Pt/\gamma\text{-}Al_2O_3$ and $Pd/\gamma\text{-}Al_2O_3$) were chosen as model reactions

$$R^1-CR^2{=}CH_2 + H_2 \longrightarrow R^1-CHR^2CH_3, \quad (4)$$

$R^1 = C_6H_5$, $R^2 = CH_3$; $R^2 = H$: $R^1 = n\text{-}C_5H_{11}$, $n\text{-}C_6H_{13}$.

To perform reactions inside an NMR magnet, a NMR-compatible reactor was designed, which allowed an increase in the temperature of the reaction zone to ~100 °C due to external heating by a hot air stream. The reaction zone and the hot-air jacket were placed in an evacuated glass Dewar to prevent overheating of gradient coils of the instrument. The catalyst is placed in the reaction zone; both the liquid reagent which is fed through a capillary and the preheated hydrogen gas which can be additionally saturated with the reagent vapour are supplied from above.

Early studies [28, 88, 148–150] addressed the spatial distribution of a liquid phase in a single cylindrical pellet of the 15% $Pt/\gamma\text{-}Al_2O_3$ catalyst in the course of hydrogenation of α-methylstyrene (AMS). At that time, one two-dimensional image was acquired during ~260 s. Nevertheless, this first experiment, where the operation of a model three-phase reactor was directly observed, revealed the presence of considerable concentration gradients of the liquid phase in the catalyst grain under conditions of the simultaneous endothermic evaporation of the liquid reactant and exothermic hydrogenation of its vapour.[88, 149, 150] Presumably, fast evaporation of the reactant occurs at the interface between the filled and dry parts of the catalyst grain, whereas its vapour is efficiently hydrogenated in the dry part of the grain.

Evidently, to study dynamic processes in a reactor, it was necessary to decrease the MR acquisition time for each image, which is determined primarily by the spin relaxation time of the liquid phase. Hence, subsequent experiments were carried out with grains of the 1 mass % $Pd/\gamma\text{-}Al_2O_3$ catalyst containing 0.1 mass % Mn.[27, 28, 85, 151, 152] This made it possible to acquire two-dimensional images in 34 s. As a result, a number of interesting dynamic processes, such as redistribution of the liquid phase in the granule upon 'ignition' of the catalyst grain, were observed. It is worthy of note that in some experiments, 'ignition' started when the pellet was virtually completely wetted and it led to drying of the grain by more than a half. Most likely, the optimal conditions for the beginning of the process are provided in the near-surface region of the grain, because the temperature directly on the surface is lower due to continuous heat removal by a gaseous reactant flow, while the diffusive transport to inner parts of the grain through pores filled with the liquid is hindered. As a result, 'ignition' begins in the grain at a particular distance from the surface, whereas the near-surface and inner regions of the grain remain filled with the liquid during a much longer period of time. As the liquid reagent is evaporated, the inner wetted region of the grain shrinks, resulting in a decrease in the rate of hydrogen transport to the evaporation – reaction zone. At a particular instant of time, inhibition becomes the main process, the temperature of the grain decreases, and a new cycle of filling of the grain with the liquid begins. Based on these results, a hypothesis can be made that hydrogenation efficiently proceeds in the region under the grain surface, where the optimal balance between the temperature of the grain and the diffusive supply of hydrogen through the pore space is provided.

In longer experiments, numerous grain 'ignitions' giving rise to quasiperiodic oscillations of the liquid that was present in the grain and the back-and-forth motion of the liquid front were observed. These oscillations were observed when the grain was filled with the liquid by more than a half and were accompanied by changes in the amount of the liquid in the grain and its temperature, large gradients of the liquid phase in the grain in the radial direction and the liquid front propagation in a radial direction. The nature of these oscillation is associated with the mutual influence of several processes, such as heat transfer, mass transfer, phase transitions and the chemical reaction itself. This is confirmed by the results of mathematical simulation.[153]

Another type of behaviour is observed when a grain is initially filled with a liquid by less than a half. In this case, the concentration wave propagation along the axis of a cylindrical grain occurs in a plug-like fashion. The largest amount of liquid was detected in the upper part of the grain, where the liquid reactant was delivered. The size of this region and its boundaries continuously oscillated. The remaining part of the grain was filled with a vapour – gas mixture and did not contain the liquid. Evaporation of AMS and the gas-phase reaction led

to temperature oscillations, which were detected in the lower dry part of the grain by a thermocouple located in this region. In the course of oscillations, the instant of time when the largest (smallest) amount of the liquid in the grain was observed did not coincide with the instant of time when the lowest (highest) temperature was detected. In addition, the amounts of the liquid in the upper and lower parts of the grain change out of phase. These observations provide evidence for the delayed feedback between the temperature of the grain and the amount of the liquid in pores.

The oscillating liquid front propagation in a catalyst grain suggests that, under particular conditions, a steady-state reaction can become unstable because of its exothermic character. Subsequent experiments demonstrated considerable sensitivity of the oscillating mode to external conditions. In particular, the existence of oscillations and their periodicity and regularity were found to depend on the activity of the catalyst, the flow rate of liquid AMS and the temperature of the supplied gas.

Experiments with single grains provide information on dynamic processes at a characteristic single-grain size scale. To study processes at larger scales and to investigate interactions and the collective behaviour of grains, experiments were performed with clusters consisting of a small number of spherical catalyst grains with a diameter of 4.2 mm, which form an approximately regular packing containing 3–4 grains in each horizontal layer. Two-dimensional MR images of horizontal sections of the grain packing were obtained. These experiments showed the possibility of 'ignition' of individual grains in a layer. These grains can act as microreactors remaining dry after 'ignition' due to the efficiency of the reaction in spite of the fact that these grains contact with grains filled with a liquid. In addition, the mutual influence of adjacent grains in the layer was revealed. In particular, it was demonstrated that dry grains can be replenished with the liquid from adjacent wet grains.

In the practice, beds consisting of a huge number of catalyst grains are used. The operation efficiency of a catalytic reactors substantially depends on the liquid phase distribution in a granular bed It is highly probable that the appearance of hot spots in a bed is also associated with the character of the liquid phase distribution. Hence, it is very important to map the liquid phase distrubution in a catalytic reactor for different operation modes. Finally, these investigations will allow establishment of the mechanisms responsible for the development of critical phenomena both at the micro- and macroscale. We carried out a series of investigations of the liquid phase distribution in a granular bed of spherical catalyst grains with a diameter of either 1 or 2–3 mm directly in the course of hydrogenation. In particular, it was found that the liquid phase distribution in a catalyst layer substantially depends on the conditions of reactor start-up. For example, essentially different liquid phase distributions are observed when a liquid reactant is supplied to a dry layer or a layer initially saturated with a liquid.

In subsequent studies, we succeeded in obviating the need for impregnation of catalyst grains with paramagnetic ions to reduce the image acquisition time. Procedures were developed for three-dimensional imaging of the whole catalyst bed with a submillimetre spatial resolution in 20–30 s and for acquiring a set of five two-dimensional sections in 2–3 s each. This, in turn, enabled us to perform the detailed study of the dynamics of the liquid phase redistribution in regular layers of spherical catalyst grains. The results of these investigations confirmed the existence of partially wet catalyst grains over long periods of time, replenishment of dry or partially wet grains with a liquid from adjacent grains and the fluctuating liquid front propagation in partially wet grain (Fig. 5). Evidently, the observation of such effects, which are impossible in a 'cold'

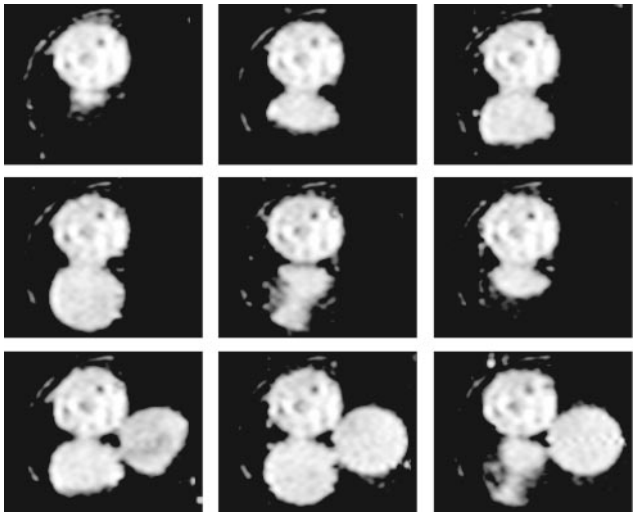


Figure 5. Liquid phase distribution in a regular bed of a catalyst (1% $Pd/\gamma\text{-}Al_2O_3$, catalyst bed diameter is 4.2 mm) directly in the course of octene hydrogenation.
Each image was acquired for 3 s at 0.5–3.5-min intervals; the images show a non-steady-state operation of the reactor; lighter shades of gray correspond to a higher local concentration of the liquid phase.

reactor (in the absence of reaction), is a manifestation of the non-linear coupling of heat and mass transfer processes, phase transformations and a chemical reaction proceeding in the reactor. In the absence of the reaction, the liquid is approximately uniformly distributed as a result of capillary imbibition of the liquid in porous grains. The above-described approaches allow individual imaging of both a liquid phase in porous grains and a liquid filling the space between grains. Experiments demonstrated that the liquid phase transport occurs primarily through film flow over the surface of catalyst grains and showed the possible disturbance of the local phase equilibrium in an exothermic reaction, which creates conditions for the reactor to deviate from a stable operation mode.[154]

Images obtained in the above-described experiments reflect the total liquid (both the reactant and the product) distribution. However, NMR is primarily a powerful spectroscopic method. Many available applications are based on a combination of NMR spectroscopy and imaging, which give either spatially localised NMR spectra, *i.e.*, spectra reflecting the local chemical composition, or tomographic images (the spatial distribution of the substance in question). These data are necessary for characterisation of the reactor operation because they provide spatially resolved information on the degree of conversion of the reactants. Undoubtedly, an improvement of combined NMR/MRI techniques for chemical engineering will be one of the main directions of further development in this field.

Unlike high-resolution NMR spectra of bulk solutions, in which the linewidth is often < 1 Hz, NMR spectra of pore-filling liquids are characterised by substantially broader lines. Nevertheless, in room-temperature NMR spectra with a spatial resolution of $2 \times 0.5 \times 0.12$ mm^3 of a mixture of AMS and cumene, which fills pores of an alumina grain, the ^{1}H linewidth is not so large, and at least semiquantitative analysis of the composition of the reaction mixture can be performed.[149] Subsequent experiments were carried out for an operating reactor with a packed bed of catalyst grains with a diameter of 1 mm.[151] In three-dimensional experiments (one spectral and two spatial coordinates), NMR spectra were measured for each element of a two-dimensional image. The reactant-to-

product ratios in different regions of the granular layer were determined directly in the course of the reaction by comparing these spectra with the spectra for pure AMS and cumene. The NMR spectrum detected in the upper part, where the liquid reactant is supplied, corresponds to virtually pure AMS; the NMR spectrum detected in the lower part, to the virtually pure product (cumene); the spectrum detected in the middle part corresponds to a mixture of the reactant and the product. Their ratio gradually changes along the height of the layer. In addition, the degree of conversion in the radial direction also varies.

A number of other catalytic reactions (liquid – solid and gas – liquid – solid) were studied by MRI. For example, esterification of methanol and acetic acid giving rise to methyl acetate and water in a reactor with a granular bed composed of small grains of the acidic form of an ion-exchange resin was documented:[155]

$$MeOH + MeCO_2H \longrightarrow MeCO_2Me + H_2O. \quad (5)$$

The spatial pattern of the degree of conversion in a reactor was obtained by combining the spectroscopic and MRI methods. It was found that the concentration of the product along the length of the reactor increases and the degree of conversion decreases as the flow rate increases. The variations of the conversion in the radial direction are as high as $\sim$20%. All experiments were carried out under stationary conditions, because the signal acquisition time was long. Later, investigations aimed at revealing correlations between the degree of conversion and the transport characteristics of the reactor with a granular bed were performed.[68, 156] For example, the plot of the local conversion *vs.* the local rate showed a good correlation between these two parameters in spite of the fact that the degree of conversion is not a local characteristic. An approach used in the studies[68, 155, 156] is based on the detection of ^{1}H NMR signals of the OH groups of acetic acid, methanol and water, which coalesce into one broadened line as a result of fast proton exchange. The position of this line in the spectrum depends on the relative concentrations of all three compounds. This approach is limited to a particular class of reactions. A more common approach, which is based on the use of MRI with a spectroscopic resolution, was successfully used[157] for catalytic esterification of propionic acid and butan-1-ol giving rise to butyl propionate and water with the use of an enzyme immobilised on a single calcium alginate grain,

$$Bu^nOH + EtCOOH \longrightarrow EtCOOBu^n + H_2O. \quad (6)$$

Experiments with the use of one spatial coordinate and one spectroscopic coordinate made it possible to trace the increase in the intensity of the signals of water and butyl propionate and the decrease in the intensity of the signal of butanol in the grain in the course of the reaction.

Multinuclear MRI produces images from not only the ^{1}H NMR signal but also from signals of other magnetic nuclei. In particular, the ^{13}C nucleus is characterised by a substantially broader range of chemical shifts than the ^{1}H nucleus, which, in principle, enables one to obtain substantially more accurate quantitative spectral information even in the case of substantial line broadening in NMR spectra. However, since the natural isotopic abundance of ^{13}C is very low (1.1%), the quality of images is poor and, consequently, a long time is required for image acquisition or it is necessary to use isotope-labelled compounds. Nevertheless, such investigations were documented. The competitive transformation of 2-methylbut-2-ene into *tert*-amyl methyl ether and *tert*-amyl alcohol at 40 °C catalysed by ion-exchange resin grains (600 – 850 μm) in a reactor with a diameter of 15 mm was studied.[158]

$$MeCH{=}CMe_2 \longrightarrow \quad (7)$$
$$\longrightarrow EtCMe_2OMe + EtCMe_2OH.$$

Two-dimensional integrated images of a reactor were acquired, and a ^{13}C NMR spectrum was measured for each element. The conversion of 2-methylbut-2-ene into ether and alcohol was found to be gradually increased in the axial direction, the selectivity to ether being retained at $\sim$75% – 80%. Both the selectivity and the conversion fluctuate in the transverse direction, the variation of the conversion for a fixed axial coordinate being $\sim$15%. The equilibrium magnetisation transfer from ^{1}H to ^{13}C nuclei was used to compensate, in part, for the loss of sensitivity in experiments with a natural isotopic abundance of ^{13}C. However, even in this case, a moderate spatial resolution (2.5×3.75 mm, without slice selection) was achieved at the acquisition time of one image of 16 h. The ^{13}C NMR signal detection was used also in investigations of hydrogenation and isomerisation of oct-1-ene.[159] To record spectra with a spatial resolution of 2.8 mm along one coordinate integrated over two other coordinates, more than a quarter of an hour was required.

In spite of considerable difficulties in performing MRI of gases and problems associated with the use of high temperatures in a probe of a microimaging instrument, some research teams designed special apparatus and proceeded to studies of high-temperature gas-phase reactions. For example, to perform MRI studies of combustion processes, a probe with water cooling and a system for removing combustion products was designed.[160] In the experiments, the behaviour of gas streams before and after methane ignition was compared. A stream of the unignited gas was visualised a flow rate of up to 2 m s^{-1} from an orifice with a diameter of 1 mm. In the presence of flame, an NMR signal gradually disappears at a distance of $\sim$3 mm from the orifice. The acquisition time of each image was several hours.

One possible way of enhancing the sensitivity in gas-phase MRI experiments is based on the use of hyperpolarised gases (see Section III). In particular, this approach was applied in studies of non-catalytic methane combustion over the surface of a granular layer of partially dehydrated zeolite NaX.[161] A mixture of hyperpolarised ^{129}Xe* and methane was supplied to the layer together with air from the bottom, and the process was studied by recording ^{129}Xe NMR spectra without spatial resolution. Due to very high sensitivity of the ^{129}Xe chemical shift to the environment, the authors succeeded in visualising different regions in the cell, which differ in the concentration of xenon, the composition of the mixture and the temperature. The exchange between these regions in the course of combustion was studied by two-dimensional exchange NMR spectroscopy.

3. Hydrogenation with parahydrogen

Hyperpolarised gases and liquids can be prepared by hydrogenation. Molecular hydrogen (H_2) is a mixture of two spin isomers, *viz.*, orthohydrogen (o-H_2, the total nuclear spin $I = 1$) and parahydrogen (p-H_2, $I = 0$). Only orthohydrogen gives an observable NMR signal due to RF-induced transitions between three spin sublevels. The spin relaxation times of the ^{1}H NMR signal under normal conditions are rather short ($T_1 = 3$ ms, $T_2 = 0.4$ ms). However, states with different multiplicities are not mixed in relaxation process, and the time of the ortho – para conversion for hydrogen under normal conditions can be as long as one year. Hence ortho- and parahydrogen can be considered as two different gases, one of which (p-H_2) is generally not involved in NMR experiments because it has the zero nuclear spin.

At room temperature, the o-H_2 : p-H_2 equilibrium ratio is close to a random value (3 : 1). At lower temperatures, the equilibrium is shifted to p-H_2. At the liquid hydrogen temperature, the equilibrium mixture consists virtually exclusively of p-H_2. At 77 K, the equilibrium ratio is approximately 1 : 1. Taking into account the low rate of spontaneous ortho – para

conversion, normal hydrogen is cooled over a catalyst for ortho–para conversion to achieve the equilibrium. Paramagnetic compounds [FeO(OH), activated carbon, *etc.*] are commonly used as catalysts for this process. An advantage of a low rate of spontaneous conversion is that, after the establishment of the equilibrium at low temperature, hydrogen can be stored at room temperature over a long period of time, no substantial changes in the o-H_2 : p-H_2 ratio being observed.

Non-equilibrium mixtures of ortho- and parahydrogen are characterised by the presence of an overall correlation of nuclear spins in an ensemble of molecules. For this correlation to be observed in NMR spectra, it is necessary to break the magnetic equivalence of nuclear spins of two hydrogen atoms. Evidently, this can be achieved by using parahydrogen in hydrogenation, as a result of which two hydrogen atoms in the reaction product are in non-equivalent positions. It is important that two atoms of one hydrogen molecule be added to one substrate molecule, which retains the initial correlation of nuclear spins. In this case, the intensity of the NMR signal of the reaction product increases by a factor of 4×10^4 for a spectrometer with a magnetic field of 7 T and this signal is even more enhanced in weak fields. The spectral manifestation of parahydrogen-induced polarisation depends on the experimental scheme. If hydrogenation is performed directly in an NMR probe, the spectrum shows two antiphase multiplets (the PASADENA effect, parahydrogen and synthesis allow dramatically enhanced nuclear alignment). If the reaction is performed in magnetic field of the Earth followed by the transfer of a sample to a probe of a spectrometer, a net enhancement of two multiplets having opposite signs is observed (ALTADENA, adiabatic longitudinal transport and dissociation engender net alignment).[162, 163]

During 15 years, hydrogenation with parahydrogen was used primarily in studies of the reaction mechanisms of homogeneous hydrogenation with transition metal complexes (for example, with the Wilkinson and Vaska catalysts). The reaction mechanism implies the formation of a metal dihydride complex as a short-lived intermediate. The use of parahydrogen in hydrogenation allows an increase in the intensity of the NMR signal by several orders of magnitude and, consequently, it is possible to detect ^{1}H NMR spectra of intermediate dihydride complexes.[164] Parahydrogen-induced polarisation was observed in homogeneous processes involving different Rh, Ir, Ru, Pt and Os complexes. Detailed studies of the kinetics and mechanism of homogeneous hydrogenation reactions involving such complexes were carried out with the use of parahydrogen as a spin label, and in some cases the new intermediate species were detected.[165–168] As a result of polarisation transfer from protons to other nuclei (^{13}C, ^{31}P, ^{15}N, ^{19}F), a much more detailed spectroscopic information can be obtained.[169–172]

Interest in the use of parahydrogen for enhancement of the NMR signal was rekindled after the publication of the study,[173] where hydrogenation with parahydrogen was used for the first time to enhance the signal in MRI. In this study, hydrogenation was followed by polarisation transfer to ^{13}C nuclei by varying the external magnetic field. Then the solution was injected into a blood vessel of a laboratory animal and an MR image was recorded. The use of this procedure and its subsequent modifications[169, 174] allowed the authors to acquire two-dimensional images of a blood vessels (angiograms) from the ^{13}C NMR signal of the reaction product in less than 1 s with a natural isotopic abundance of ^{13}C.

The presence of a catalyst in solution is a drawback of the approach used in the studies,[169, 173, 174] which substantially limits its application in studies of living organisms and makes it impossible to perform these investigations in medical purposes. In addition, this fact hampers the development of technical applications of MRI. For example, the construction of systems with a continuous polarised fluid (liquid or gas) flow for MRI of different objects with the use of homogeneous hydrogenation requires large amounts of an expensive catalyst. In principle, the catalyst can be removed from solution with an appropriate adsorbent.[175] However, the polarisation relaxation time is equal to a few seconds and is additionally decreased in the case of a contact between the product and a porous material.

Up to 2007, data on parahydrogen-induced polarisation in heterogeneous reactions were lacking. It should be noted that polarisation was observed [176] when performing hydrogenation on colloidal $(Pd)_x[N(n\text{-}C_8H_{17})_4Cl]_y$ particles in a liquid. However, it cannot be ruled out that the solution simultaneously contained the dissolved metal complex, which was responsible for the observed polarisation. In addition, the authors of this study mentioned the commonly accepted view that polarisation of the product is impossible in heterogeneous catalytic hydrogenation with parahydrogen. Actually, many industrial hydrogenation catalysts are highly dispersed metal (Pt or Pd) particles deposited on a porous support (for example, Al_2O_3). It is commonly accepted that hydrogenation on these catalysts involves dissociative chemisorption of hydrogen on metal particles, hydrogen migration over the particle surface and spillover onto the support. Under these conditions, the probability that the correlation of nuclear spins of the starting parahydrogen molecule will be retained and that two hydrogen atoms of one H_2 molecule will be present in one product molecule is negligibly small. Hence, until recently, it was believed that parahydrogen-induced polarisation can be observed only in homogeneous catalytic processes with all attendant problems and drawbacks.

In recent years, experts in catalysis have made great efforts to establish bridges between homogeneous and heterogeneous catalytic processes.[177] In many cases, homogeneous catalysts exhibit much higher activity and selectivity; however, the unbeatable advantage of heterogeneous catalysts is that the latter can easily be removed from the reaction mixture. Presently, the latter fact is of key importance not only in view of strengthening of environmental requirements for industrial processes, but also because the catalysts become considerably more expensive as their structure gets progressively more complex. In this connection, a combination of the advantages of homogeneous and heterogeneous catalysis by immobilisation of homogeneous catalysts on an appropriate porous support is one of increasing trends in modern catalysis.[178, 179] Nowadays, several procedures are available for immobilisation based on formation of hydrogen bonds, ion pairs, covalent attachment to organic or inorganic supports, *etc.* Many of these procedures were used also in the design of new hydrogenation catalysts [180–185] characterised by high stability, efficiency and selectivity in heterogeneous hydrogenation under mild conditions. It is important that, in many cases, the chemical structure of metal complexes does not undergo substantial changes upon their immobilisation. Consequently, the reaction mechanism presumably remains unchanged upon immobilisation. However, it is difficult to obtain direct evidence for this fact.

Polarisation in heterogeneous hydrogenation with parahydrogen was observed for the first time in the study by Koptyug *et al.*[186] (Fig. 6). For this purpose the following three catalysts were used: the Wilkinson catalyst (**1**) immobilised on a styrene–divinylbenzene copolymer (**1**/polymer), the same catalyst immobilised on modified silica gel $RhCl(PPh_3)_2PPh_2(CH_2)_2-SiO_2$ (**1**/SiO_2) and the immobilised tridentate complex $Rh(cod)(sulfos)-SiO_2$ (**2**/SiO_2; cod is cycloocta-1,5-diene; sulfos is $^-O_3S(C_6H_4)CH_2C(CH_2PPh_2)_3$). In one series of experiments, hydrogenation was carried out in magnetic field of an NMR spectrometer. For this purpose, a tube with a solution of the substrate (styrene) and the catalyst

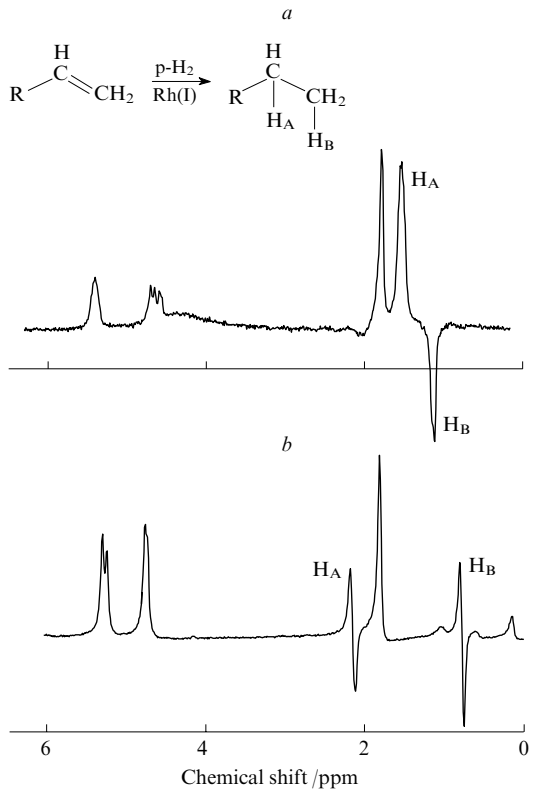


Figure 6. Parahydrogen-induced polarisation of nuclear spins in heterogeneous hydrogenation of unsaturated compounds.
(*a*) ALTADENA for propylene hydrogenation (R = Me) in weak field at 130 °C, (*b*) PASADENA for styrene hydrogenation (R = Ph) in strong field at 60 °C. In both cases, equilibrium NMR signals of the reaction product are negligibly small.

(**1**/SiO_2 or **1**/polymer) was placed in a probe of the spectrometer and heated to 65–80 °C. Both catalysts efficiently hydrogenate styrene to ethylbenzene. In reactions with the use of enriched parahydrogen, both catalysts lead to substantial polarisation of nuclear spins in the reaction product and give rise to the characteristic antiphase structure of multiplets in the NMR spectrum (PASADENA, see Fig. 6 *b*). The NMR spectra of the product, which was prepared by hydrogenation outside a magnet followed by the transfer of the sample to a probe of an NMR spectrometer, show multiplets with net polarisation of opposite signs (ALTADENA). It was also found that after removal of the catalyst from the solution, bubbling with hydrogen did not lead to either the formation of the product or polarisation. These results confirm that polarisation upon hydrogenation with parahydrogen was observed in a heterogeneous process for the first time.

Besides, hydrogenation with parahydrogen was applied for the first time [186] to generate nuclear spin polarisation in gases. For this purpose, catalysts immobilised on a porous support (**1**/SiO_2 or **2**/SiO_2) were used. To observe the PASADENA effect, the tube with a dry catalyst was placed in an NMR probe and heated to 80 °C. A mixture of propylene and enriched parahydrogen was continuously introduced into a tube through thin capillaries. The nuclear spin polarisation of the reaction product, *viz*., propane, was determined from NMR spectra. To observe the ALTADENA effect, the reaction was carried out outside a magnet. For this purpose, a mixture of propylene and enriched parahydrogen was continuously purged through a copper tube packed with a catalyst heated to 130 °C and then passed to an NMR probe (see Fig. 6 *a*). The observation of polarisation upon hydrogenation of a gas is unambiguous evidence for the fact that nuclear spin polarisation can be produced not only in homogeneous but also in heterogeneous processes. Later, polarisation in hydrogenation of propylene with parahydrogen was achieved with the use of the silica gel-immobilised $RhCl(POMe_3)_3$ complex.

In further investigations,[187] the possibility of the preparation of a hyperpolarised gas in heterogeneous hydrogenation was used for MR imaging of model objects; NMR tubes with cross-shaped partitions or capillary bundles mounted inside the tubes were used as such objects. As in the earlier experiments,[186] hydrogenation of propylene was performed using a continuous flow of a gas mixture through a heated catalyst. Then the polarised product (propane) was delivered through a system of tubes to the model object, and the MR image was obtained by detecting the NMR signal of the polarised gas. Until recently, the preparation of hyperpolarised gases was limited primarily by laser polarisation of noble gases (see Section III). Therefore, the results of the studies [186, 187] substantially extended the range of gases, for which the signal-to-noise ratio in MRI experiments can be substantially improved by producing nuclear spin polarisation.

The above-described results are of importance for several reasons. First, the observation of polarisation of the product with the use of parahydrogen is direct evidence for the pair-wise addition of two hydrogen atoms of an H_2 molecule to one substrate molecule. Therefore, these results confirm that the reaction mechanism of hydrogenation by metal complexes remains unchanged upon their immobilisation onto a support. Second, the pair-wise addition is a necessary but not sufficient condition for observation of polarisation. After the formation of the dihydride complex, two hydrogen atoms become non-equivalent and their spin correlation decays due to spin relaxation.[188] Immobilisation of the complex leads to a substantial decrease in molecular mobility, and the spin relaxation times can be substantially shorter than the spin relaxation times of complexes in solution. The observation of polarisation indicates that the lifetime of intermediate dihydride cannot be substantially longer than its spin relaxation time.

The preparation of pure fluids with polarised nuclear spins opens a broad spectrum of new possible applications, particularly, those associated with the NMR signal detection in low and ultra-low magnetic fields,[189, 190] where the equilibrium differences in the populations of spin energy sublevels are very small. The possibility of creating continuous flows of polarised fluids is particularly attractive. This possibility was exemplified by heterogeneous hydrogenation of propylene. Efficiency of biomedical experiments with parahydrogen-induced polarisation can be increased using solid catalysts. In addition, many studies based on homogeneous hydrogenation with parahydrogen are characterised by an uncertain duration of this process because the termination of bubbling of a solution with parahydrogen does not lead to the immediate termination of the reaction. This substantially complicates the interpretation of the results.[170, 191] It is important to obtain pure quantum states in experiments with the use of parahydrogen-induced polarisation aimed at designing quantum computers.[192, 193]

In view of the results of recent investigations, hydrogenation with parahydrogen has yet another important potential application in NMR. Many modern NMR and MRI experiments are based on the creation of particular perturbation of a spin system, which then undergoes evolution over a particular period of time. The evolution is followed by the 'read-out' of the new state of the spin system. This principle provides the basis for the diffusion coefficient and flow rate measurements,[139, 194] different two-dimensional NMR spectroscopic experiments,[195] *etc*. If the evolution period is substantially longer than the spin relaxation times, the detection of the final state of the spin system does not give useful information on the

processes in question. Hence, until recently, researchers have believed that the maximum evolution time is comparable with the spin–lattice relaxation time (T_1) of the spin system. However, recently it has been demonstrated [196, 197] that this limitation can be overcome by using the unique properties of singlet spin states. Actually, for pairs of equivalent nuclei with spin 1/2, the states with a certain total spin of the pair are the eigenstates of the Hamiltonian: singlet ($I = 0$) and triplet ($I = 1$). This is also the case with a hydrogen molecule (see above). The spinless singlet state is not involved in relaxation processes which affect the NMR spectra, and the interconversion time between states with different total spins can be longer that the spin relaxation times by an order of magnitude or larger.[196, 197] As in the above-considered NMR of parahydrogen, the singlet state of a pair of nuclei is not directly involved in NMR experiments. Hence, to use the unique properties of singlet states, it is necessary to construct a molecular system in which the magnetic equivalence of a pair of nuclei could be 'switched on' and 'switched off' under the external action on the spin system. So far, the two different ways of performing this switching have been suggested: the physical transfer of a sample from a weak magnetic field to a strong field and back [197] or prolonged RF irradiation of the spin system in a strong field of a spectrometer.[196] For example, the measured lifetime of the singlet state (T_s) of 2,3-dibromothiophene in DMSO-d_6 in weak field was 104 s ($T_1 = 17$ s).[197] For 2-chloroacrylonitrile in DMSO-d_6, $T_s = 141$ s ($T_1 = 7.8$ s) in the case of continuous RF irradiation.[196]

Practical outputs of these investigations hold considerable promise. A substantial increase in the lifetime of spin coherence can be useful in studies of slow transport processes. For example, the use of long-lived singlet states in experiments on measurements of molecular diffusion coefficients (D) by PFG NMR at $T_s = 10\,T_1$ allows a decrease of the lower detection limit of D by an order of magnitude, all other factors being the same. An example of the application of this approach was described in the study,[198] where the diffusion coefficients of 2-chloroacrylonitrile in a DMSO-d_6–D_2O mixture were measured in the temperature range from -46 to $+25$ °C. Long-lived spin states hold promise also in investigations of very slow dynamic processes, such as chemical exchange, conformational transformations, protein and RNA refolding, *etc*. Two-dimensional exchange spectroscopy with the use of long-lived singlet states was proposed in the study.[199] This study dealt with conformational transformations of monosaccharide, in which all hydrogen atoms, except for two atoms, were replaced by deuterium. The lifetime of the singlet state for this pair of protons was demonstrated to be 37 times longer than T_1. In an exchange experiment, the mixing time allotted for a conformational change of the molecules was 12 s ($T_1 = 0.7$ s).

The extensive development of the theory of long-lived spin states is presently underway.[200–204] Evidently, the use of states with lifetimes substantially longer than T_1 also shows promise for imaging applications, particularly, for liquid and gas flows, for example in the remote imaging (see Section III). A combination of the properties of long-lived singlet states and nuclear polarisation produced by hydrogenation with parahydrogen is also promising.[170, 191] The initially produced state of a pair of nuclear spins in the reaction product is singlet, and an additional advantage is that an excess of these states in an ensemble of molecules increases by several orders of magnitude.

V. Conclusion

In recent years, the number of studies in the area of physicochemical applications of the MRI technique has rapidly increased. In addition to a substantial extension of the range of objects and processes, the MRI technique itself underwent considerable changes. This stage of investigations is characterised by the development of new applications, which have been considered to be impossible to implement in practice until recently. These are studies of solids without the use of solid-state NMR techniques, investigations of gas transport, studies of high-temperature reactions, *etc*. In addition, the development of methods of nuclear spin hyperpolarisation and spectroscopy of singlet spin states opens new prospects for the further progress in MRI.

We thank our colleagues engaged in these investigations and particularly our co-authors working at the Boreskov Institute of Catalysis of the Siberian Branch of the Russian Academy of Sciences. The research has been performed with the financial support of the Russian Foundation for Basic Research (Project No. 05-03-32 472), the Division of Chemistry and Materials Science of the Russian Academy of Sciences (Project Nos 5.2.3 and 5.1.1), the Siberian Branch of the Russian Academy of Sciences (Integration Grant 11), the Programme for State Support of Leading Scientific Schools of the Russian Federation (Grant NSh-4821.2006.3), the Russian Science Support Foundation (I V Koptyug and A A Lysova), the Council on Grants of the President of the Russian Federation (Grant MK-5135.2007.3) and the Global Energy Foundation (A A Lysova).

References

1. *NMR Imaging in Chemical Engineering* (Eds S Stapf, S Han) (Weinheim: Wiley-VCH, 2005)
2. *Appl. Magn. Reson. (Special Issue)* **32** 1 (2007)
3. L F Gladden *AIChE J.* **49** 2 (2003)
4. M D Mantle, A J Sederman *Prog. Nucl. Magn. Reson. Spectrosc.* **43** 3 (2003)
5. I V Koptyug, R Z Sagdeev *Usp. Khim.* **71** 672 (2002) [*Russ. Chem. Rev.* **71** 593 (2002)]
6. I V Koptyug, R Z Sagdeev *Usp. Khim.* **71** 899 (2002) [*Russ. Chem. Rev.* **71** 789 (2002)]
7. I V Koptyug, R Z Sagdeev *Usp. Khim.* **72** 183 (2003) [*Russ. Chem. Rev.* **72** 165 (2003)]
8. P Blumler, B Blumich *Rubber Chem. Technol.* **70** 468 (1997)
9. B Blumich, P Blumler, K Saito, in *Solid State NMR of Polymers. Studies in Physical and Theoretical Chemistry* Vol. 84 (Eds I Ando, T Asakura) (Amsterdam: Elsevier, 1998) p. 123
10. J R Moore, L Garrido, J L Ackerman *Ceram. Eng. Sci. Proc.* **11** 1302 (1990)
11. J L Ackerman, L Garrido, J R Moore, B Pfleiderer, Y Wu, in *Magnetic Resonance Microscopy. Methods and Applications in Materials Science, Agriculture and Biomedicine* (Eds B Blumich, W Kuhn) (Weinheim: VCH, 1992) p. 237
12. M S Conradi *J. Magn. Reson.* **93** 419 (1991)
13. W S Veeman, in *Magnetic Resonance Microscopy. Methods and Applications in Materials Science, Agriculture and Biomedicine* (Eds B Blumich, W Kuhn) (Weinheim: VCH, 1992) p. 29
14. S Matsui, M Nonaka, T Nakai, T Inouye *J. Magn. Reson.* **138** 220 (1999)
15. P J McDonald, B Newling *Rep. Prog. Phys.* **61** 1441 (1998)
16. E W Randall, in *Encyclopedia of Nuclear Magnetic Resonance* Vol. 9 (Eds D M Grant, R K Harris) (Chichester: Wiley, 2002) p. 150
17. P Bodart, T Nunes, E W Randall *Solid State NMR* **8** 257 (1997)
18. V S Swaminathan, B H Suits *J. Magn. Reson.* **132** 274 (1998)
19. S Choi, X-W Tang, D G Cory *Int. J. Imaging Syst. Technol.* **8** 263 (1997)
20. I V Mastikhin, B J Balcom, P J Prado, C B Kennedy *J. Magn. Reson.* **136** 159 (1999)
21. C B Kennedy, B J Balcom, I V Mastikhin *Can. J. Chem.* **76** 1753 (1998)
22. G R Davies, D J Lurie, J M S Hutchison, S J McCallum, I Nicholson *J. Magn. Reson.* **148** 289 (2001)
23. J B Miller *Prog. Nucl. Magn. Reson. Spectrosc.* **33** 273 (1998)

24. V Antochshuk, M-J Kim, A K Khitrin *J. Magn. Reson.* **167** 133 (2004)
25. M J Kim, A K Khitrin *Magn. Reson. Imaging* **23** 865 (2005)
26. I V Koptyug, D R Sagdeev, E Gerkema, H Van As, R Z Sagdeev *J. Magn. Reson.* **175** 21 (2005)
27. I V Koptyug, A A Lysova, R Z Sagdeev, V A Kirillov, A V Kulikov, V N Parmon *Catal. Today* **105** 464 (2005)
28. I V Koptyug, A A Lysova, in *NMR Imaging in Chemical Engineering* (Eds S Stapf, S Han) (Weinheim: Wiley-VCH, 2005) p. 570
29. I V Koptyug, A A Lysova *Bruker Spin Rep.* **157**–**158** 22 (2006)
30. I V Koptyug, A V Khomichev, A A Lysova, R Z Sagdeev *Appl. Magn. Reson.* (2007) (in the press)
31. D D Laws, H M L Bitter, A Jerschow *Angew. Chem., Int. Ed.* **41** 3096 (2002)
32. F H Larsen, H J Jakobsen, P D Ellis, N C Nielsen *J. Magn. Reson.* **131** 144 (1998)
33. P R Bodart, J-P Amoureux, Y Dumazy, R Lefort *Mol. Phys.* **98** 1545 (2000)
34. W Wlodarczyk, R Boroschewski, M Hentschel, P Wust, G Monich, R Felix *J. Magn. Reson. Imaging* **8** 165 (1998)
35. D German, P Chevallier, A Laurent, H Saint-Jalmes *Magn. Reson. Mater. Phys., Biol. Med.* **13** 47 (2001)
36. K P Nott, L D Hall *Trends Food Sci. Technol.* **10** 366 (1999)
37. N Hosten, R Felix, P Wust, W Wlodarczyk, M Hentschel, R Noeske, H Rinneberg *Phys. Med. Biol.* **44** 607 (1999)
38. S J Doran, T A Carpenter, L D Hall *Rev. Sci. Instrum.* **65** 2231 (1994)
39. D Hauck, P Blumler, B Blumich *Macromol. Chem. Phys.* **198** 2729 (1997)
40. B H Suits, D White *J. Appl. Phys.* **60** 3772 (1986)
41. J Goetz, K Zick, C Heinen, T Koenig *Chem. Eng. Process.* **41** 611 (2002)
42. C Heinen, J Tillich, H Buggisch, T Zeiser, H Freund *Magn. Reson. Imaging* **23** 369 (2005)
43. M L Johns, A J Sederman, A S Bramley, L F Gladden, P Alexander *AIChE J.* **46** 2151 (2000)
44. A Feinauer, S A Altobelli, E Fukushima *Magn. Reson. Imaging* **15** 479 (1997)
45. T W J Scheenen, D van Dusschoten, P A de Jager, H Van As *J. Magn. Reson.* **142** 207 (2000)
46. T W J Scheenen, F J Vergeldt, C W Windt, P A de Jager, H Van As *J. Magn. Reson.* **151** 94 (2001)
47. B R Locke, M Acton, S J Gibbs *Langmuir* **17** 6771 (2001)
48. U Tallarek, T W J Scheenen, H Van As *J. Phys. Chem. B* **105** 8591 (2001)
49. A J Sederman, M D Mantle, C Buckley, L F Gladden *J. Magn. Reson.* **166** 182 (2004)
50. J D Seymour, S L Codd, E L Gjersing, P S Stewart *J. Magn. Reson.* **167** 322 (2004)
51. B C Hoskins, L Fevang, P D Majors, M M Sharma, G Georgiou *J. Magn. Reson.* **139** 67 (1999)
52. K Potter, R L Kleinberg, F J Brockman, E W McFarland *J. Magn. Reson., Ser. B* **113** 9 (1996)
53. G Gonzalez-Gil, P N L Lens, A Van Aelst, H Van As, A I Versprille, G Lettinga *Appl. Environ. Microbiol.* **67** 3683 (2001)
54. B Manz, F Volke, D Goll, H Horn *Biotechnol. Bioeng.* **84** 424 (2003)
55. K P Nott, M Paterson-Beedle, L E Macaskie, L D Hall *Biotechnol. Lett.* **23** 1749 (2001)
56. M Paterson-Beedle, K P Nott, L E Macaskie, L D Hall *Methods Enzymol.* **337** 285 (2001)
57. E E Beuling, D van Dusschoten, P Lens, J C van den Heuvel, H Van As, S P P Ottengraf *Biotechnol. Bioeng.* **60** 283 (1998)
58. E L Gjersing, S L Codd, J D Seymour, P S Stewart *Biotechnol. Bioeng.* **89** 822 (2005)
59. S P Wolfe, E Hsu, L M Reid, J M Macdonald *Biotechnol. Bioeng.* **77** 83 (2001)
60. P E Thelwall, A A Neves, K M Brindle *Biotechnol. Bioeng.* **75** 682 (2001)
61. C Planchamp, M K Ivancevic, C M Pastor, J-P Vallee, S Pochon, F Terrier, J M Mayer, M Reist *Biotechnol. Bioeng.* **85** 656 (2004)
62. P N L Lens, M A Hemminga *Biodegradation* **9** 393 (1998)
63. H Van As, P Lens *J. Ind. Microbiol. Biotechnol.* **26** 43 (2000)
64. L F Gladden *Top. Catal.* **24** 19 (2003)
65. A J Sederman, L F Gladden *Chem. Eng. Sci.* **56** 2615 (2001)
66. L F Gladden, M D Mantle, A J Sederman, E H L Yuen *Appl. Magn. Reson.* **22** 201 (2002)
67. L F Gladden, M H M Lim, M D Mantle, A J Sederman, E H Stitt *Catal. Today* **79** 203 (2003)
68. L F Gladden, P Alexander, M M Britton, M D Mantle, A J Sederman, E H L Yuen *Magn. Reson. Imaging* **21** 213 (2003)
69. M D Mantle, A J Sederman, L Gladden *Chem. Eng. Sci.* **56** 523 (2001)
70. M H M Lim, A J Sederman, L F Gladden, E H Stitt *Chem. Eng. Sci.* **59** 5403 (2004)
71. L D Anadon, M H M Lim, A J Sederman, L F Gladden *Magn. Reson. Imaging* **23** 291 (2005)
72. N L Nguyen, V van Buren, A von Garnier, E H Hardy, R Reimert *Chem. Eng. Sci.* **60** 6289 (2005)
73. A J Sederman, M D Mantle, L F Gladden *J. Magn. Reson.* **161** 15 (2003)
74. M D Mantle, A J Sederman, L F Gladden, S Raymahasay, J M Winterbottom, E H Stitt *AIChE J.* **48** 909 (2002)
75. J J Heras, A J Sederman, L F Gladden *Magn. Reson. Imaging* **23** 387 (2005)
76. A J Sederman, M D Mantle, L F Gladden *Magn. Reson. Imaging* **21** 359 (2003)
77. A A Khrapitchev, S Han, S Stapf, B Blumich *J. Magn. Reson.* **159** 36 (2002)
78. I Okamoto, S Hirai, K Ogawa *Meas. Sci. Technol.* **12** 1465 (2001)
79. I V Koptyug, L Yu Ilyina, A V Matveev, R Z Sagdeev, V N Parmon, S A Altobelli *Catal. Today* **69** 385 (2001)
80. L G Kaiser, J W Logan, T Meersmann, A Pines *J. Magn. Reson.* **149** 144 (2001)
81. I V Koptyug, S A Altobelli, E Fukushima, A V Matveev, R Z Sagdeev *J. Magn. Reson.* **147** 36 (2000)
82. E Brunner, M Haake, L Kaiser, A Pines, J A Reimer *J. Magn. Reson.* **138** 155 (1999)
83. S Tsushima, S Hirai, Y Yamamoto, Y Nakasuji *Magn. Reson. Imaging* **21** 430 (2003)
84. B Newling, C C Poirier, Y Zhi, J A Rioux, A J Coristine, D Roach, B J Balcom *Phys. Rev. Lett.* **93** 154503-1 (2004)
85. I V Koptyug, A A Lysova, A V Matveev, R Z Sagdeev, V N Parmon *Katal. Prom-sti* (Spec. Issue) 60 (2004)
86. I V Koptyug, A V Matveev, S A Altobelli *Appl. Magn. Reson.* **22** 187 (2002)
87. S L Codd, S A Altobelli *J. Magn. Reson.* **163** 16 (2003)
88. I V Koptyug, A A Lysova, A V Matveev, L Yu Ilyina, R Z Sagdeev, V N Parmon *Magn. Reson. Imaging* **21** 337 (2003)
89. R W Mair, R L Walsworth *Appl. Magn. Reson.* **22** 159 (2002)
90. K Knagge, J Prange, D Raftery *Chem. Phys. Lett.* **397** 11 (2004)
91. R Seydoux, A Pines, M Haake, J A Reimer *J. Phys. Chem. B* **103** 4629 (1999)
92. G E Pavlovskaya, Z I Cleveland, K F Stupic, R J Basaraba, T Meersmann *Proc. Natl. Acad. Sci. USA* **102** 18275 (2005)
93. R W Mair, R Wang, M S Rosen, D Candela, D G Cory, R L Walsworth *Magn. Reson. Imaging* **21** 287 (2003)
94. A Wong-Foy, S Saxena, A J Moule, H-M L Bitter, J A Seeley, R McDermott, J Clarke, A Pines *J. Magn. Reson.* **157** 235 (2002)
95. M Mossle, S-I Han, W R Myers, S-K Lee, N Kelso, M Hatridge, A Pines, J Clarke *J. Magn. Reson.* **179** 146 (2006)
96. A J Moule, M M Spence, S-I Han, J A Seeley, K L Pierce, S Saxena, A Pines *Proc. Natl. Acad. Sci. USA* **100** 9122 (2003)
97. J A Seeley, S Han, A Pines *J. Magn. Reson.* **167** 282 (2004)
98. E E McDonnell, S-I Han, C Hilty, K L Pierce, A Pines *Anal. Chem.* **77** 8109 (2005)
99. C Hilty, E E McDonnell, J Granwehr, K L Pierce, S-I Han, A Pines *Proc. Natl. Acad. Sci. USA* **102** 14960 (2005)
100. E Fukuishima, in *NMR Imaging in Chemical Engineering* (Eds S Stapf, S Han) (Weinheim: Wiley-VCH, 2005) p. 490
101. E Fukushima *Adv. Complex Syst.* **4** 503 (2001)
102. A C Rees, J F Davidson, J S Dennis, P S Fennell, L F Gladden, A N Hayhurst, M D Mantle, C R Muller, A J Sederman *Chem. Eng. Sci.* **61** 6002 (2006)

103. P S Fennell, J F Davidson, J S Dennis, L F Gladden, A N Hayhurst, M D Mantle, C R Muller, A C Rees, S A Scott, A J Sederman *Chem. Eng. Sci.* **60** 2085 (2005)
104. R Savelsberg, D E Demco, B Blumich, S Stapf *Phys. Rev. E* **65** 020301 (2002)
105. S Harms, S Stapf, B Blumich *J. Magn. Reson.* **178** 308 (2006)
106. R Wang, M S Rosen, D Candela, R W Mair, R L Walsworth *Magn. Reson. Imaging* **23** 203 (2005)
107. R Wang, M S Rosen, D Candela, R W Mair, R L Walsworth *Chem. Eng. Technol.* **23** 203 (2005)
108. A Caprihan, E Fukushima, A D Rosato, M Kos *Rev. Sci. Instrum.* **68** 4217 (1997)
109. X Yang, D Candela *Phys. Rev. Lett.* **85** 298 (2000)
110. X Y Yang, C Huan, D Candela, R W Mair, R L Walsworth *Phys. Rev. Lett.* **88** 44301 (2002)
111. C Huan, X Y Yang, D Candela, R W Mair, R L Walsworth *Phys. Rev. E* **69** 41302 (2004)
112. D M Mueth, G F Debregeas, G S Karczmar, P J Eng, S R Nagel, H M Jaeger *Nature (London)* **406** 385 (2000)
113. D M Mueth *Phys. Rev. E* **67** 011304 (2003)
114. M T Hardin, T Howes, D A Mitchell, A K Whittaker *Biotechnol. Lett.* **24** 521 (2002)
115. K M Hill, A Caprihan, J Kakalios *Phys. Rev. Lett.* **78** 50 (1997)
116. K M Hill, A Caprihan, J Kakalios *Phys. Rev. E* **56** 4386 (1997)
117. G Metcalfe, L Graham, J Zhou, K Liffman *Chaos* **9** 581 (1999)
118. I V Koptyug, L Yu Ilyina, A V Matveev, V N Parmon, R Z Sagdeev *Khim. Fiz.* **21** 68 (2002) [a]
119. A V Matveev, L V Barysheva, I V Koptyug, V M Khanaev, A S Noskov *Chem. Eng. Sci.* **61** 2394 (2006)
120. A F McDowell, M S Conradi, J Haase *J. Magn. Reson., Ser. A* **119** 211 (1996)
121. Y Cheng, Q L Huang, M Eic, B J Balcom *Langmuir* **21** 4376 (2005)
122. L Pel, K Kopinga, E F Kaasschieter *J. Phys. D: Appl. Phys.* **33** 1380 (2000)
123. F D Cano, T W Bremner, R P McGregor, B J Balcom *Cem. Concr. Res.* **32** 1067 (2002)
124. I V Koptyug, L Yu Khitrina, Yu I Aristov, M M Tokarev, K T Iskakov, V N Parmon, R Z Sagdeev *J. Phys. Chem. B* **104** 1695 (2000)
125. A A Lysova, I V Koptyug, R Z Sagdeev, V N Parmon, J A Bergwerff, B M Weckhuysen *J. Am. Chem. Soc.* **127** 11916 (2005)
126. J A Bergwerff, L G A van der Water, A A Lysova, I V Koptyug, T Visser, K P de Jong, B M Weckhuysen *Stud. Surf. Sci. Catal.* **162** 175 (2006)
127. L Yu Khitrina, I V Koptyug, N A Pakhomov, R Z Sagdeev, V N Parmon *J. Phys. Chem. B* **104** 1966 (2000)
128. Yu I Aristov, N N Bukhavtsova, N V Vernikovskaya, V P Voloshin, V N Glaznev, L Yu Ilyina, I V Koptyug, Yu G Korobeinikov, I N Korotkikh, V A Luchnikov, N N Medvedev, N M Ostrovskii, V N Parmon, A D Simonov, M M Tokarev, V B Fenelonov, V M Fomin, N A Chumakova, N A Yazykov *Sovremennye Podkhody k Issledovaniyu i Opisaniyu Protsessov Sushki Poristykh Tel* (Modern Approaches to Investigation and Description of the Drying of Porous Solids) (Ed. V N Parmon) (Novosibirsk: Siberian Branch of the Russian Academy of Sciences, 2001)
129. I V Koptyug, L Yu Khitrina, V N Parmon, R Z Sagdeev *Magn. Reson. Imaging* **19** 531 (2001)
130. J A Bergwerff, T Visser, B R G Leliveld, B D Rossenaar, K P de Jong, B M Weckhuysen *J. Am. Chem. Soc.* **126** 14548 (2004)
131. Z R Ismagilov, S A Yashnik, A V Matveev, I V Koptyug, J A Moulijn *Catal. Today* **105** 484 (2005)
132. *Oscillations and Travelling Waves in Chemical Systems* (Eds R J Field, M Burger) (New York: Wiley, 1985)
133. Y Gao, A R Cross, R L Armstrong *J. Phys. Chem.* **100** 10159 (1996)
134. A L Cross, R L Armstrong, C Gobrecht, M Paton, C Ware *Magn. Reson. Imaging* **15** 719 (1997)
135. M M Britton *J. Phys. Chem. A* **107** 5033 (2003)
136. M M Britton *J. Phys. Chem. A* **110** 2579 (2006)
137. I V Koptyug, A A Lysova, A V Matveev, V N Parmon, R Z Sagdeev *Top. Catal.* **32** 83 (2005)
138. I V Koptyug, A A Lysova, V N Parmon, R Z Sagdeev *Kinet. Katal.* **44** 436 (2003) [b]
139. J Kärger, D M Ruthven *Diffusion in Zeolites and Other Microporous Solids* (New York: Wiley, 1992)
140. A Toth, K Showalter *J. Chem. Phys.* **103** 2058 (1995)
141. O Steinbock, P Kettunen, K Showalter *J. Phys. Chem.* **100** 18970 (1996)
142. M Kaern, M Menzinger *J. Phys. Chem. B* **106** 3751 (2002)
143. M Kaern, M Menzinger *J. Phys. Chem. A* **106** 4897 (2002)
144. M M Britton, A J Sederman, A F Taylor, S K Scott, L F Gladden *J. Phys. Chem. A* **109** 8306 (2005)
145. R Evans, C R Timmel, P J Hore, M M Britton *Chem. Phys. Lett.* **397** 67 (2004)
146. V V Zhivonitko, I V Koptyug, R Z Sagdeev *J. Phys. Chem. A* (2007) (in press)
147. *Nuclear Magnetic Resonance. A Specialist Periodical Report* Vol. 33 (Cambridge: RSC Publishing, 2004)
148. I V Koptyug, A V Kulikov, A A Lysova, V A Kirillov, R Z Sagdeev, V N Parmon *Dokl. Akad. Nauk* **385** 205 (2002) [c]
149. I V Koptyug, A V Kulikov, A A Lysova, V A Kirillov, V N Parmon, R Z Sagdeev *J. Am. Chem. Soc.* **124** 9684 (2002)
150. I V Koptyug, A V Kulikov, A A Lysova, V A Kirillov, V N Parmon, R Z Sagdeev *Chem. Sust. Dev.* **11** 109 (2003)
151. I V Koptyug, A A Lysova, A V Kulikov, V A Kirillov, V N Parmon, R Z Sagdeev *Appl. Catal. A* **267** 143 (2004)
152. I V Koptyug, A A Lysova, A V Kulikov, V A Kirillov, V N Parmon, R Z Sagdeev *Magn. Reson. Imaging* **23** 221 (2005)
153. V A Kirillov, I V Koptyug, A V Kulikov, N A Kuzin, A A Lysova, A B Shigarov, V N Parmon *Teor. Osnovy Khim. Tekhnol.* **39** 27 (2005) [d]
154. V A Kirillov, I V Koptyug *Ind. Eng. Chem. Res.* **44** 9727 (2005)
155. E H L Yuen, A J Sederman, L F Gladden *Appl. Catal. A* **232** 29 (2002)
156. E H L Yuen, A J Sederman, F Sani, P Alexander, L F Gladden *Chem. Eng. Sci.* **58** 613 (2003)
157. M Kuppers, C Heine, S Han, S Stapf, B Blumich *Appl. Magn. Reson.* **22** 235 (2002)
158. B S Akpa, M D Mantle, A J Sederman, L F Gladden *Chem. Commun.* 2741 (2005)
159. A J Sederman, M D Mantle, C P Dunckley, Z Huang, L F Gladden *Catal. Lett.* **103** 1 (2005)
160. P M Glover, B Newling, C Poirier, B J Balcom *J. Magn. Reson.* **176** 79 (2005)
161. S Anala, G E Pavlovskaya, P Pichumani, T J Dieken, M D Olsen, T Meersmann *J. Am. Chem. Soc.* **125** 13298 (2003)
162. J Natterer, J Bargon *Prog. Nucl. Magn. Reson. Spectrosc.* **31** 293 (1997)
163. S B Duckett, C J Sleigh *Prog. Nucl. Magn. Reson. Spectrosc.* **34** 71 (1999)
164. C R Bowers, D P Weitekamp *J. Am. Chem. Soc.* **109** 5541 (1987)
165. P Hubler, J Bargon *Angew. Chem., Int. Ed.* **39** 3701 (2000)
166. J P Dunne, S Aiken, S B Duckett, D Konya, K Q A Lenero, E Drent *J. Am. Chem. Soc.* **126** 16708 (2004)
167. C R Bowers, in *Encyclopedia of Nuclear Magnetic Resonance* Vol. 9 (Eds D M Grant, R K Harris) (Chichester: Wiley, 2002) p. 750
168. S B Duckett, S A Colebrooke, in *Encyclopedia of Nuclear Magnetic Resonance* Vol. 9 (Eds D M Grant, R K Harris) (Chichester: Wiley, 2002) p. 598
169. H Johannesson, O Axelsson, M Karlsson *C. R. Phys.* **5** 315 (2004)
170. T Jonischkeit, U Bommerich, J Stadler, K Woelk, H G Niessen, J Bargon *J. Chem. Phys.* **124** 201109-1 (2007)
171. S Aime, R Gobetto, F Reineri, D Canet *J. Chem. Phys.* **119** 8890 (2003)
172. L T Kuhn, U Bommerich, J Bargon *J. Phys. Chem. A* **110** 3521 (2006)
173. K Golman, O Axelsson, H Johannesson, S Mansson, C Olofsson, J S Petersson *Magn. Reson. Med.* **46** 1 (2001)
174. M Goldman, H Johannesson, O Axelsson, M Karlsson *Magn. Reson. Imaging* **23** 153 (2005)

175. P Bhattacharya, K Harris, A P Lin, M Mansson, V A Norton, W H Perman, D P Weitekamp, B D Ross *Magn. Reson. Mater. Phys., Biol. Med.* **18** 245 (2005)
176. A Eichhorn, A Koch, J Bargon *J. Mol. Catal. A* **174** 293 (2001)
177. *Catalysis by Metal Complexes. Catalyst Separation, Recovery and Recycling. Chemistry and Process Design* Vol. 30 (Eds D J Cole-Hamilton, R P Tooze) (Dordrecht: Springer, 2006)
178. P Barbaro, C Bianchini *Top. Catal.* **19** 17 (2002)
179. D J Cole-Hamilton *Science* **299** 1702 (2003)
180. C Bianchini, D G Burnaby, J Evans, P Frediani, A Meli, W Oberhauser, R Psaro, L Sordelli, F Vizza *J. Am. Chem. Soc.* **121** 5961 (1999)
181. C Merckle, S Haubrich, J Blumel *J. Organomet. Chem.* **627** 44 (2001)
182. C P Mehnert, E J Mozeleski, R A Cook *Chem. Commun.* 3010 (2002)
183. J Huang, T Jiang, B Han, T Mu, Y Wang, X Li, H Chen *Catal. Lett.* **98** 225 (2004)
184. C Simons, U Hanefeld, I W Arends, A J Minnaard, T Maschmeyer, R A Sheldon *Chem. Commun.* 2830 (2004)
185. P Barbaro, C Bianchini, G Giambastiani, W Oberhauser, L M Bonzi, F Rossi, V Dal Santo *Dalton Trans.* 1783 (2004)
186. I V Koptyug, K V Kovtunov, S R Burt, M S Anwar, C Hilty, S Han, A Pines, R Z Sagdeev *J. Am. Chem. Soc.* **129** 5580 (2007)
187. L-S Bouchard, K V Kovtunov, S R Burt, M S Anwar, I V Koptyug, R Z Sagdeev, A Pines *Angew. Chem., Int. Ed.* **46** 4064 (2007)
188. G Buntkowsky, B Walaszek, A Adamczyk, Y Xu, H-H Limbach, B Chaudret *Phys. Chem. Chem. Phys.* **8** 1929 (2006)
189. S Xu, V V Yashchuk, M H Donaldson, S M Rochester, D Budker, A Pines *Proc. Natl. Acad. Sci. USA* **103** 12668 (2006)
190. R McDermott, S-K Lee, B ten Haken, A H Trabesinger, A Pines, J Clarke *Proc. Natl. Acad. Sci. USA* **101** 7857 (2004)
191. D Canet, S Bouguet-Bonnet, C Aroulanda, F Reineri *J. Am. Chem. Soc.* **129** 1445 (2007)
192. P Hubler, J Bargon, S J Glaser *J. Chem. Phys.* **113** 2056 (2000)
193. M S Anwar, D Blazina, H A Carteret, S B Duckett, J A Jones *Chem. Phys. Lett.* **400** 94 (2004)
194. P T Callaghan *Principles of Nuclear Magnetic Resonance Microscopy* (Oxford: Clarendon Press, 1991)
195. R R Ernst, G Bodenhausen, A Wokaun *Principles of Nuclear Magnetic Resonance in One and Two Dimensioms* (Oxford: Clarendon Press, 1987)
196. M Carravetta, M H Levitt *J. Am. Chem. Soc.* **126** 6228 (2004)
197. M Carravetta, O G Johannessen, M H Levitt *Phys. Rev. Lett.* **92** 153003 (2004)
198. S Cavadini, J Dittmer, S Antonijevic, G Bodenhausen *J. Am. Chem. Soc.* **127** 15744 (2005)
199. R Sarkar, P R Vasos, G Bodenhausen *J. Am. Chem. Soc.* **129** 328 (2007)
200. M Carravetta, M H Levitt *J. Chem. Phys.* **122** 214505 (2005)
201. G Pileio, M Concistre, M Carravetta, M H Levitt *J. Magn. Reson.* **182** 353 (2006)
202. K Gopalakrishnan, G Bodenhausen *J. Magn. Reson.* **182** 254 (2006)
203. R Kimmich, D E Demco, S Hafner, in *Magnetic Resonance Microscopy. Methods and Applications in Materials Science, Agriculture and Biomedicine* (Eds B Blumich, W Kuhn) (Weinheim: VCH, 1992) p. 59
204. N Lugeri, F De Luca, B Maraviglia, in *Magnetic Resonance Microscopy. Methods and Applications in Materials Science, Agriculture and Biomedicine* (Eds B Blumich, W Kuhn) (Weinheim: VCH, 1992) p. 103

[a] — *Chem. Phys. Rep. (Engl. Transl.)*
[b] — *Kinet. Catal. (Engl. Transl.)*
[c] — *Dokl. Phys. Chem. (Engl. Transl.)*
[d] — *Theor. Found. Chem. Eng. (Engl. Transl.)*